Failure mechanisms in lithium silicon batteries

F.Q. de Boer

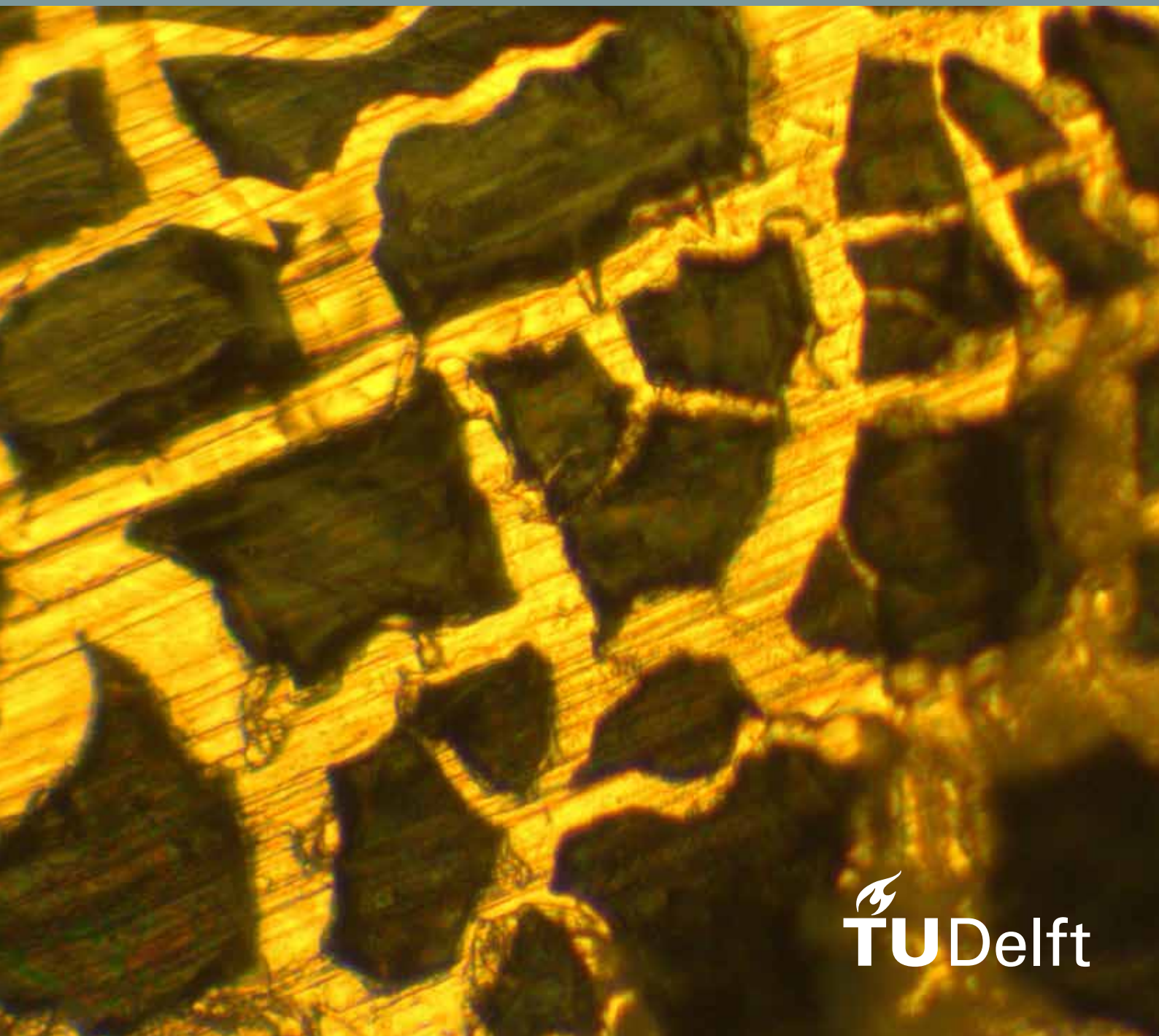

TU Delft

Failure mechanisms in lithium-silicon batteries

by

F.Q. de Boer

in partial fulfilment of the requirements for the degree of

Bachelor of Science
in Applied Physics

at the Delft University of Technology,

Student number:	4141342
Project duration:	April 21, 2015 – July 24, 2015
Supervisor:	Prof. dr. H.W. Zandbergen
Instructor:	M.Tech. S. Basak
Examiners:	Prof. dr. H.W. Zandbergen and Dr. ir. F.D. Tichelaar

National Centre for High Resolution Electron Microscopy (NCHREM)

Cover image: silicon on copper foil sample after discharging to 0 V, 1000× magnified

TU Delft Delft University of Technology

Abstract

Lithium silicon (Li-Si) batteries offer more than ten times the theoretical specific capacity compared to current lithium ion battery technologies, by using a silicon anode. In practice however, the cycle life of Li-Si batteries is very limited. The large volume change of the silicon anode is known to be the main reason for this. Research on the volume changes during varying cell cycles and voltages is presented in this thesis and an experimental set up for a quasi in situ study of the SEI layer is suggested.

Cycling tests with an amorphous silicon thin film of 220 nm deposited using magnetron sputtering on a copper foil current collector confirmed that the major cause of capacity loss is swelling of the silicon during lithiation, causing the silicon to detach from the current collector and resulting in significant capacity loss. Increasing the lower cut off voltage from 0 V to 0.2 V resulted in a slight improvement of cycle life. Silicon detachment also decreased as determined by SEM images. EFTEM and EDX mapping showed a clear split between a partially lithiated silicon layer on the surface and a pure silicon layer on the current collector side. It can be concluded that discharging Li-Si batteries to 0.2 V instead of 0 V is a promising method to reduce the swelling of silicon during lithiation.

Contents

Acknowledgements

Shibabrata (Shiv) Basak, my instructor during this project, was a fantastic instructor, going far beyond what was required in instructing me. Without all his efforts in arranging alternatives and working over hours to gather results, I would have never finished the project on time. Therefore I would like to thank him for all his effort, including but not limited to taking SEM images at 10 pm, spending dozens of hours preparing and imaging samples for this research and asking his friends and contacts for help and advice on difficulties encountered in this research.

I would like to thank Professor Henny Zandbergen for his enthusiasm and interest in this project and for providing invaluable suggestions where Shiv and I struggled.

Tom de Kruijff was very helpful in teaching me how to use lab equipment and giving advice on sample preparation methods. Whenever a weird clamp or instrument was needed, he was able to find it.

Sarmila Dutta kindly deposited silicon in her own time for this project, allowing me to start experimenting with the important silicon on copper foil sample without further delays.

And finally I would like to thank all the kind people of the HREM group who provided helpful advice, friendly greetings and interesting presentations of their own work.

1

Introduction

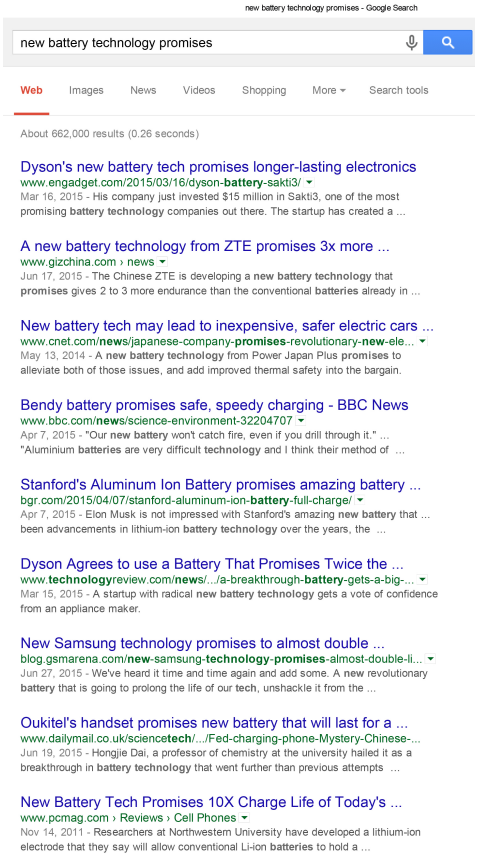

Figure 1.1: Popular media have reported numerous revolutional improvements in battery technologies, but so far none of these have been commercialized.

In the 20 years since their first commercial usage, lithium-ion batteries have conquered the world and are used in almost every mobile phone, laptop and in electric vehicles (EVs). Without the lithium-ion battery, mobile devices wouldn't be as powerful as they are, whilst being lightweight and compact. However, especially recently, battery technology seems to be holding back new generations of mobile phones and EVs, which consumers expect to use a full day without intermediate charging. Unfortunately, the year on year successive technology improvements in semiconductors, as described by Moore's law, do not apply to battery technology.

> "The basic reasons why an emerging technology may not follow Moore's Law is either because we tend to underestimate the complexity of the system to which the technology is applied, or we underestimate the basic principles of physics and chemistry which would inherently constrain a Moore-type breakthrough in that field."
> - Ashutosh Jogalekar, *Scientific American Blogs* (2013)[1]

Given the huge incentives for developing a revolution in batteries, it is no wonder that the number scientists working in this field is increasing rapidly. Even mainstream media follow research on batteries, with stories about a supposed new breakthrough in battery development appearing monthly. Besides all this attention given to research on battery technology, the field of batteries is very interesting in itself, being on the crossroads of physics, chemistry, electrical engineering, material sciences and many more disciplines. All of this with very clear goals in mind, including, but not limited to, making batteries safer, more sustainable, of higher capacity, have better cycle life, allow faster charging.

In the following sections some background information on lithium batteries will be presented, to explain the reader the state of current lithium battery technology and to explain the incentives behind this research.

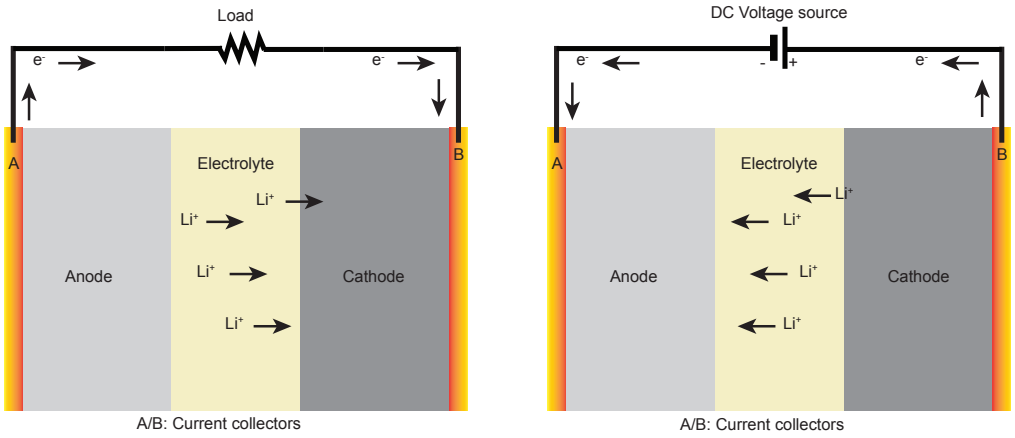

Figure 1.2: Schematics of a discharging (left) and a charging lithium-ion battery.

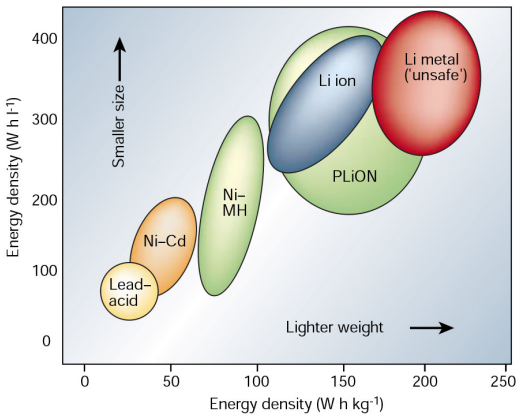

Figure 1.3: This graph illustrates the energy density of lithium ion batteries compared to some common battery technologies available on the market. Source: Tarascon and Armand [3]

1.1. Lithium ion batteries

Lithium batteries have only been around since the late 1970s, for specialized purposes, with rechargeable lithium ion batteries not becoming available until more than a decade later.[2] The reasons for lithium to be used in batteries lie in it's high energy density[3], high electrical potential material and it's low self-discharge rate. First the operating principle and main components of a lithium ion battery are described, followed be a concise history of lithium ion batteries.

1.1.1. Operating principle and components

Lithium ion batteries are based on a reversible process of insertion and extraction of lithium ions in a host material. During discharge, lithium is inserted, and during charge, lithium is extracted. This process is a reaction between two electrodes, separated by electrolyte. The host material is located in one of the electrodes, called the anode. The other electrode, which is the source of lithium ions, is called the cathode. A schematic battery is shown in figure 1.2.

The lithium insertion and extraction process is a redox reaction of the host material. One of the characteristics of a redox reaction is the transport of electrons. The electrolyte between the electrodes does not allow transport of electrons, so the electrons are led external from the battery between the electrodes. The electrons can enter and exit the electrodes through the current collectors, which are attached to the external circuit.[4][5]

1.2. Silicon battery electrodes

Even though today's commercial lithium ion based batteries already have one of the highest energy densities of any kind of commercially available battery (see figure 1.3), this can still be improved a lot by using different anode materials than the currently most used one, graphite. The best candidate to replace graphite is probably silicon. A lithium ion battery with a silicon anode (Li-Si battery) could theoretically increase the anode energy density tenfold compared to a conventional graphite electrode. Working Li-Si batteries have been studied in the lab for more than a decade, but are not ready to be commercialized yet.

The problem with silicon electrodes in practice is their bad cycle life of generally less than 50 cycles in current lab-built batteries.[3] Research on Li-Si batteries is therefore focused on improving the cycle life. Some of the phenomena that cause the lacking cycle life are the large volume change (up to 320%) of the silicon electrode during discharge - causing mechanical stress and loss of electrical contact - and the formation of an unstable solid electrolyte interphase layer (SEI layer) - a layer on the silicon surface which is formed by electrolyte reacting with the silicon electrode.[6]

1.3. History of lithium-ion batteries

The development of rechargeable lithium-ion batteries started with the description of intercalation - the reversible insertion of lithium (ions) in layered materials - by Whittingham[7][8]. This resulted in early lithium batteries, using a TiS_2/Li cell. A problem in this cell was the lithium electrode, which formed long dendrite structures across the electrolyte, causing internal short circuits which would lead to ignition of the battery. Eventually, this cell chemistry was therefore abandoned.

One of the key people in the development of lithium batteries is John B. Goodenough, who was involved in the development of the currently still most used cathode materials $LiCoO_2$[9] and $LiFePO_4$ in the 1980s.[10][i] In 1991, Sony Corporation was the first to develop a commercial lithium ion battery, used in one of their camcorders.[12] This means that latest commercially used battery chemistry is more than two decades old, which feels like a century in the field of modern electronics.

Silicon anodes have only been researched in university research labs since the late 1990s[13], but have not been commercialized yet. A Stanford University spin off company has produced large batches of lithium-silicon/carbon composite batteries, offering a more modest capacity doubling at best, but these are still only for testing purposes.[14]

1.4. Research goal

In this thesis the lithiation and delithiation behaviour and swelling effects of the silicon electrode in Li-Si batteries are researched and explained, to find out which mechanisms in the silicon electrode cause Li-Si batteries to fail. Using electron microscopy and spectroscopy the electrode's properties at different points in the battery cycle are documented to confirm that silicon indeed behaves like the existing literature and theory describes, and previously unknown behaviour is described and explained where possible.

[i] Goodenough who is aged 92 as of 2015, has not retired, but still works in his lab at the University of Texas to find another breakthrough in lithium battery chemistry.[11]

2

Theory

Background information on lithium batteries will be discussed in this chapter, such as the operating principle, battery components, challenges, materials, devices for testing batteries. The observation techniques used in the experiments are also explained. Having gone through the operating principle of the lithium ion battery in the introduction, the components and main properties of a battery will be discussed more in depth in the following sections. This will help the reader to understand the experiment and interpret the experimental results.

2.1. Capacity

For most purposes the capacity is the most important property of a battery. How much charge a battery can store is usually given in Ampère-hours (Ah). The capacity of a battery can be calculated from a discharge current plot (current vs. time) using:

$$Q = \int_{t_0}^{t_{empty}} I(t)\mathrm{dt} \tag{2.1}$$

where Q denotes the battery capacity and t_0, t_{empty} are the starting time when the battery is 100% charged and the time where the battery voltage has reached cut off voltage respectively. I is the discharge current in amperes. To find the energy E a battery stores, the capacity is integrated over the voltage:

$$E = \int_{t_0}^{t_{empty}} Q \quad dV \tag{2.2}$$

2.1.1. Charging and discharging

A fully charged lithium battery will have all the lithium located in the anode. When discharging, electron transport is allowed through the external circuit and a load, which triggers lithium ions to travel from anode to cathode, where they are inserted in the cathode host material and recombined with the electrons. This process can continue until the anode is depleted of lithium or until the cathode is fully inserted with lithium, at which point the battery is empty.

When charging a battery, an external current is applied transporting electrons in the reverse direction, which extracts the lithium from the cathode and transports it back to the anode. Once no more lithium can be extracted from the cathode, the battery is fully charged.

The charge/discharge rate of a battery is usually expressed as the C-rate, where a C-rate of 1C means that the battery can safely be fully charged or discharged in an hour, a C-rate of 0.5 means that it takes two hours two hours to charge the battery and a battery rated at 5C can be fully charged or discharged in 12 minutes. A rate of 1C is fairly typical for commercial lithium batteries. [15]

For safety purposes, the charge and discharge rate is limited in commercial batteries by an electronic safety circuit. Discharging or charging a battery too quickly produces a lot of heat [16] - creating a potential fire - and greatly reduces cycle life of the battery. The charge and discharge rate of lithium

batteries is limited compared to capacitors due to the fact that charge is stored in bulk volumes in batteries, whereas capacitors store charge on surfaces. The rate of inserting or extracting ions from a bulk material is limited by path length, electrical conductivity of the electrode material and by the diffusion coefficient of lithium ions in the electrode.[17][18] Because of these properties, nano-scale cathode materials have better performance: the path length is small, the distance to the current collector is small, resulting in better conductivity, and the diffusion coefficient is better, with more surface area present.

2.1.2. Galvanostat

A galvanostat is a device that keeps a constant current flowing to or from a battery cell and log the cell voltage in the meantime.[19] The constant current is accomplished by using a variable internal resistance, as follows from Coulombs law:

$$\mathrm{I}_0 = \mathrm{U}/\mathrm{R}_{\mathrm{variable}} \tag{2.3}$$

Where I_0 is the desired current draw, U the voltage of the battery and $\mathrm{R}_{\mathrm{variable}}$ the variable resistance in the galvanostat. To be able to draw pico ampere range currents from a 3V cell, the internal resistance of the device must be very high.

2.2. Voltage

The open circuit voltage of a battery cell is determined by the electrochemical potentials of the anode and cathode[6]:

$$V = \frac{\mu_{anode} - \mu_{cathode}}{e} \tag{2.4}$$

With V denoting the voltage in Volts, μ the respective electrochemical potentials (energy/mole) and e the number of electrons transported per reaction. The values of the chemical potentials are a subject of chemistry and can be assumed constant for pure electrode material. A higher voltage allows a battery to do more work, i.e. allow a higher peak power draw. According to the electric power law:

$$P = VI \tag{2.5}$$

with P being the power in Watt and I the current draw.

2.3. Battery components

In this section various materials and forms for the main battery components will be discussed and compared to motivate a choice for the experimental battery's components.

2.3.1. Cathode

The cathode in a lithium battery has to accommodate the lithium ions during discharging - *lithiation* - and release the ions during charging - *delithiation*. This process requires both chemical and physical structural integrity of the material. The process also has to be reversible with acceptable efficiency, as a consequence of this, suitable cathode materials store lithium between layers of the host material, without changing the lattice structure of it. This is called intercalation. Commonly used anode materials are $LiMnO_2$, $LiCoO_2$ and $LiFePO_4$.

2.3.2. Electrolyte

The electrolyte is one of the most important components in a battery, ensuring transport of lithium ions and preventing direct transport of electrons between the electrodes. Furthermore, the stability of the electrolyte is an important factor in the safety, cycle life and (dis)charge properties of a battery. The requirements that an electrolyte should fulfil are well worded by Aurbach *et al.*[20]:

> "they should have a large electrochemical window in order to be compatible with [the] 4 V cathodes, they have to be as non-volatile and non-poisonous as possible and yet provide reasonable conductivity at a wide temperature range, and they should induce on the carbon material a surface chemistry which leads to the formation of passivating surface films."

A large electrochemical window means that the material does not decompose at the voltage range used in the battery (and it is better to use a higher voltage so more energy can be stored). In equation

form this is expressed as[21] (see also figure **??**):

$$eV_{oc} = \mu_A - \mu_C \leq E_G \tag{2.6}$$

with e representing the electron charge, V_{oc} the battery's open circuit voltage, μ_A, μ_C the anode and cathode material's chemical potential respectively and E_G the electrolyte's electrochemical windows. The passivating surface films will be discussed in section 2.3.3.

Because lithium ions have to be able to travel through the electrolyte during cycling, lithium salts should be soluble in the electrolyte and shouldn't react with the electrolyte (this also means that the electrolye is a liquid in most cases).[6] Ethylene carbonate (EC) and other carbonates such as dimethyl carbonate (DMC), diethyl carbonate (DEC) and ethyl-methyl carbonate (EMC) are suitable for this.[22] Because EC is not a good ionic (lithium ion) conductor, lithium salts are not very well soluble in DMC, a combination of these is used. The total solution will be referred to as EC-DMC, EC-DEC or EC-EMC respectively.

The electrolyte reacts with water, so handling it requires a controlled environment such as a glove-box. [i] The $LiPF_6$ salt - which is dissolved in the electrolyte - is sensitive to moisture and will react with water to form HF acid[23][24]. HF is a strong acid that dissolves oxides.

2.3.3. Anode

The anode of a lithium-ion battery is what contains the lithium when the battery is charged. It is possible to use pure lithium metal as an anode material, but for commercial purposes this is too dangerous. Lithium forms so called dendrites on its surface in a battery. Dendrites are long structures 'growing' perpendicular on the electrode surface. They form by lithium reacting with the electrolyte. After many cycles the dendrite reaches through the separator and touches the anode, resulting in a short circuit. This will overheat the battery, causing fire.

To prevent dendrite formation, lithium is stored in host materials such as graphite (LiC_6). The disadvantage is that charge density decreases from 3862 mAh $g^{-}1$ to 372 mAh $g^{-}1$.[23] For a lab-built battery in a monitored environment, lithium metal can be used relatively safely though if the battery is not cycled hundreds or times.

The theoretical specific capacity of a battery in mAh/g is given by:

$$q = \frac{nF}{3.6 \cdot M} \tag{2.7}$$

with n being the number of free electrons per charge carrier ion, F is Faraday's constant (9.649 C/mol), and M the molecular weight of the lithiated cathode material (e.g. $LiFePO_4$). Using this equation the theoretical capacities for different anode materials can be calculated. For example for $Li_{4.4}Si$:

$$q = \frac{4.4 \cdot 9.65 \times 10^4 \mathrm{C/mol}}{3.6 \cdot 28\mathrm{u}} = 4200\mathrm{mAh/g} \tag{2.8}$$

Capacity values for some possible anode materials are shown in table 2.1. The net capacity for the best current commercial li-ion batteries is around 100 mAh/g.[25]

Material	Spec. cap. (mAh/g)	Volume change
LiC_6	372	10%
$Li_{13}Sn_5$	990	252%
Li_9Al_4	2235	604%
$Li_{22}Si_5$	**4200**	**320%**

Table 2.1: Theoretical specific capacities for some electrode materials and the volumetric change in percent that they undergo after lithiation.[4][5][23][26] Of these, only LiC_6 is currently used in commercial batteries.

As the anode material is lithiated and delithiated, the structure, volume, mechanical and thermodynamic properties change. For some anode materials the volume changes to several times the original volume during lithiation. The volumetric change is of most influence on the cycle life.

[i] A glovebox is a sealed box with an air lock to insert specimen and rubber gloves to manipulate them, the gas (often nitrogen or argon) inside the box is kept seperated from the outside air.

The extent of the volumetric change (also called *swelling*) can be roughly predicted from the number of lithium ions that will bind with a anode molecule. Given that for a silicon and carbon anode during discharge $Li_{4.4}Si$ and LiC_6 form respectively, one can already predict that the volumetric change of a lithium electrode battery will be larger. The exact volumetric changes (swelling) are more difficult to determine, being a dependent on the change of the lattice structure.[26] The literature values of volume expansion are given in table 2.1. High swelling causes contact loss with the current collector resulting in increased resistance and isolated electrode particles, reducing the battery capacity.[27]

SEI layer

The cathode of a battery is separated from the electrolyte by thin layer (100 nm) which is formed by electrode material reacting with the electrolyte. This layer is called the solid electrolyte interphase layer (SEI layer). For most li-ion batteries, the SEI will only appear at the anode, since it is generally unstable at the battery operating potential,[28].

The SEI layer in lithium-based batteries is formed on the cathode mainly during the first couple of charge-discharge cycles.[29] This formation happens alongside the battery (dis)charge reactions. The SEI layer is impenetrable for the electrolyte, but lithium ions can travel through it, therefore, once the SEI layer is formed, the material behind it is not in direct contact with the electrolyte any more, and the SEI layer does not grow.[30] Thus, an equilibrium situation has been reached where the SEI layer protects the electrode material behind it from further reacting with the electrolyte. This also means however, that this process is irreversible. The thickness, shape, density and other properties of the SEI layer are dependent on properties such as the electrolyte used, the battery potential and the form of the electrode surface.[31] When using a graphite anode, the SEI layer works exactly as described above, protecting the anode surface from the electrolyte. When using a silicon anode however, the swelling of up to 302% cracks the SEI layer open, exposing the silicon to electrolyte. Once the exposed spots have reacted and the battery is cycled again, the SEI layer will crack open again, therefore the SEI layer is unstable on silicon. During multiple cycles, the amount of material (including lithium) stuck in the SEI is enough to result in significant capacity loss.[32 33 34]

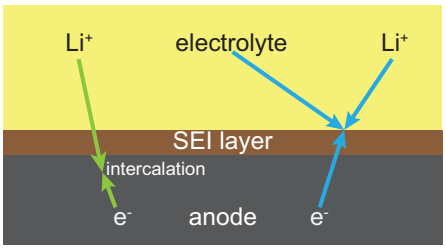

Figure 2.1: Simple representation of the SEI layer formation process (right), happening side-by-side with the 'normal' intercalation reaction (left). (Image based on Pinson and Bazant[28])

There is some uncertainty regarding the definition of the SEI layer, since there have been few direct observations of it. It was found that the SEI layer consists of two layers with different densities and chemistries.[35 36] Most (older) research does not mention this difference, which makes it questionable which part of the SEI layer was actually observed. The measured thickness of the SEI layer varies depending on the number of cycles, the anode material and what cycling settings are used.[28] Values from literature range roughly from 10 nm to 100 nm (see table 2.2).

For the conventional graphite anode, research has shown that the SEI layer on amorphous silicon consists of "hydrocarbons, lithium alkyl carbonates, LiOH, Li_2CO_3 and Li_2O" (source: McArthur *et al.*[37]). Khan *et al.*[38] have shown that the same materials are present in the SEI layer on silicon nanowire electrodes. But according to Nie *et al.*[39] the SEI on silicon nanoparticles mainly consists of lithium ethylene dicarbonate, LiF and LixSiOy. It is certain however, that the SEI layer mostly consists of decomposed electrolyte material.

Thickness (nm)	Electrode material and type	Electrolyte	Reference
40	Silicon nanowires	EC-DEC	Khan *et al.*[38]
110	Silicon nanotubes		Wu *et al.*[32]
45-90	$LiFePO_4$		Li *et al.*[31]
15	$LiMn_2O_4$ thin film	EC-DMC	Lei *et al.*[40]
90	Graphite powder	EC-DMC	Andersson *et al.*[41]

Table 2.2: Some SEI layer thickness observations, showing a relatively wide range of values found.

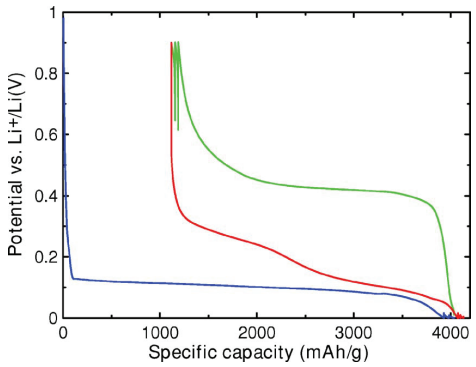

Figure 2.2: Typical Li-Si battery discharge V/t curve. The blue line is the first discharge, the green line the first charge and the red line the second discharge. Notice the flat plateau for the blue curve below 0.2 V and another plateau for the green line at 0.4 V. (source: Li and Dahn [42])

Electrode shape and appearance

To reduce the effect of some of the issues that are limiting practical lithium-silicon batteries, such as the volume change and resulting current collector detachment, the silicon electrode can be implemented in several appearances, such as nano-structured silicon, amorphous silicon, thin film deposited silicon or crystalline silicon.[43]

The shape of the electrode can dramatically affect cycle life. Silicon nanowire electrodes have been reported to achieve hundreds[44] or even thousands of cycles[32] without dramatic capacity loss, whereas amorphous silicon electrodes start to fail after just 10 cycles.[13,45] However, for commercial batteries, nanowires have several disadvantages. It is expensive to manufacture nanowires, and mass production of silicon nanowires is still subject of research. Growing nanowires on a suitable current collector such as copper is not possible, with workaround being needed. The packing density of nanowires is also inherently less than that of amorphous silicon, due to the void space between the nanowires. And finally, it is expected that solid electrolytes will be used in future batteries. Combining this with the fragile nanowires will come with new challenges.

To make silicon thin films, silicon wafers might seem like a good source, being readily available from the semiconductor industry, and made from high grade crystalline silicon. It may seem convenient to etch these wafers into any desired electrode shape using lithography. However, crystalline silicon is unsuitable for batteries because of its poor lithiation and delithiation abilities. The diffusion rate of lithium is 10-100 times less in crystalline silicon compared to amorphous silicon.[46] More importantly, during lithiation, crystalline silicon changes into the amorphous phase. If the silicon is lithiated further up to its fully lithiated state ($Li_{4.4}Si$) it will become a crystalline again, but now paired with lithium.[47] Part of this phenomena can be seen in figure 2.2 as the plateau. The plateau indicates the existence of an equilibrium between amorphous and crystalline lithiated silicon (Li_xSi) phases. Around 50 mV, phase changes between amorphous and crystalline lithiated silicon occur.[42] Starting with an amorphous sample, a discharge to 0 V can therefore still form crystalline lithiated silicon. The formation of crystalline lithiated silicon is partially irreversible because of its poor lithium diffusion - lithium ions cannot be drawn from the inside of a bulk layer. This irreversibility results in capacity loss, with both lithium and silicon being taken out from the battery cycle. Making extremely thin electrodes to counter this is not a good option, because it decreases the battery capacity, with more weight of current collector and other passive material needed relative to the active battery components.

The phase change is also suggested to cause inhomogeneous swelling of the silicon, increasing the mechanical stress on the electrode.[4] In general, amorphous silicon has been found to withstand much higher stresses without fracturing than crystalline silicon can.[48]

2.3.4. Current collector

A current collector should above all have good conductivity. Furthermore, it also needs to add rigidity to the electrodes, since materials like lithium and silicon deform permanently under pressure.

Because the current collector doesn't contribute the the charge and energy that the battery can store, it is desirable to use a lightweight and thin material so that the energy density of the battery is impacted less. For batteries available for consumers, cost is also an important measure. And the

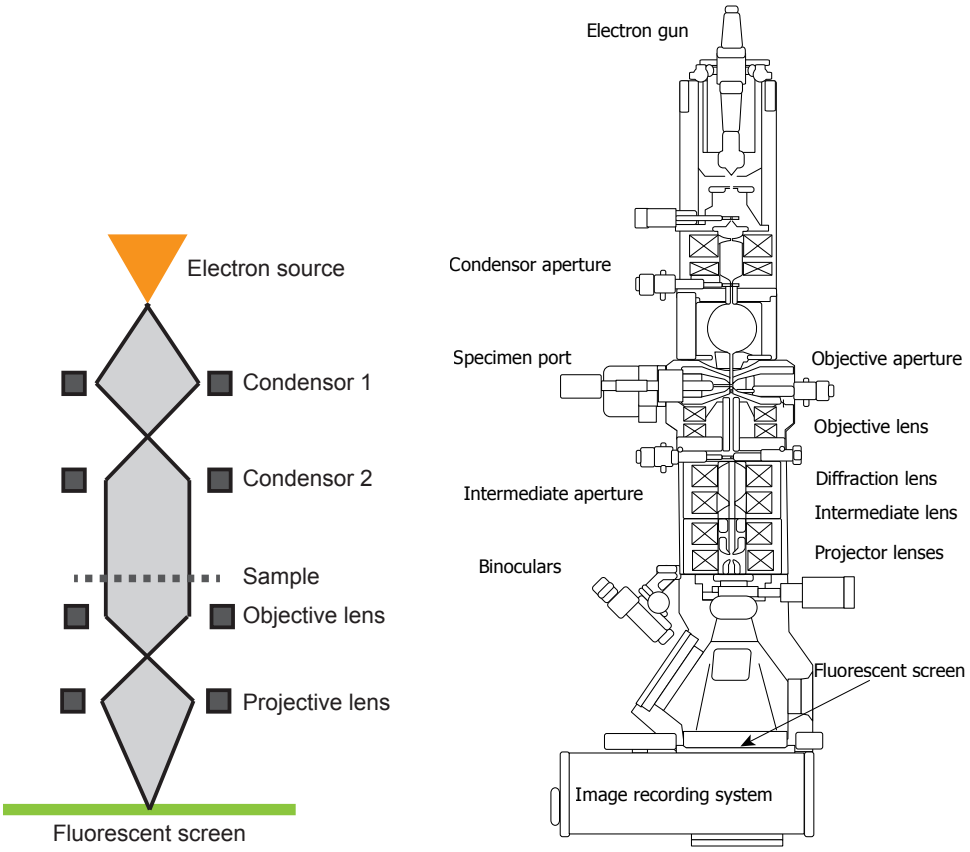

Figure 2.3: Left: Ray diagram for bright field TEM imaging, showing the rays being transmitted by the sample. Right: Section diagram of a typical TEM with the main components labeled. Image source: Wikimedia Commons [50]

current collector should be stable and resistant against the corrosive conditions in a battery.[49] This depends on the electrochemical potential of the current collector material, which should be higher than the potential of the cathode. Some examples of current collector materials are copper, nickel, steel and gold.[23]

2.4. Observing electrode behaviour

To view the effects of lithiating thin film silicon electrodes, samples will have to be observed at one of the smallest scales while also obtaining quantitative information. The best method to do these observations is TEM (transmission electron microscopy) observation because it can be paired with spectroscopic analysing instruments in the same machine and allows characterising of what is inside the SEI layer rather than just its surface. TEM works quite similar to optical microscopy. An electron gun at the top (see 2.3) fires electrons to the bottom. The entire column is kept under high vacuum, because air particles would deflect the electrons. Using electromagnets as lenses, the electrons can be focused and deflected. The fluorescent screen on the bottom makes the electrons visible for the human eye. Images can also be captured by a digital camera. Since the electron beam has to be *transmitted* through the sample, the sample has to be very thin (less than 1 µm). But the benefit of using electrons instead of light is the higher resolution that can be reached, with the disadvantage of being limited to gray scale images. There is also a risk of the electrons damaging the sample during observation. In the next paragraphs TEM techniques used in the experiments are described.

2.4.1. Bright field TEM

Bright field (BF) TEM observation makes use of the direct electron beam, similar to a conventional light microscope. The electron beam is sent through the sample - which therefore has to be very thin - and is focused below the sample on a screen or camera (see figure 2.3). Objects that do not transmit

electrons will appear dark, void space will appear light. BF TEM gives useful information about the internal structure of thin samples.

2.4.2. Electron diffraction

The electron beam of a TEM can be used for diffraction. The main patterns that diffraction may produce are spots and rings. If bright spots, in a repeating structure, are visible in the diffraction pattern, then the sample contains macroscopic crystals. Concentric rings without any bright spots are a sign of a completely amorphous sample structure. Combinations between these are possible.[51]

2.4.3. EDX

Energy-dispersive X-ray spectroscopy (EDX) is a technique to identify which elements a sample contains, determined by the specific X-ray peaks emitted by every element. By focusing the electron beam of the TEM on a single spot on the sample, atoms on that spot in the sample are excited and will emit X-ray radiation.[52] The wavelength of these X-rays will depend on corresponding excited states, which are different for every element. EDX analysis is usable mostly for higher elements (atom number Z higher than 3), since the lower elements have less excited states to distinguish. Because the beam has to be focused in one spot, EDX is limited to spot analysis. However, using software which performs automated EDX spectroscopy in a fine grid of spots, it is possible to perform 2D EDX spectroscopy. The main limitation of EDX is that it cannot detect light elements such as H, He and Li, because these elements do not emit detectable levels of X-ray radiation when excited.[52]

2.4.4. EFTEM

Energy-filtered transmission electron microscopy (EFTEM) fills the gap where EDX falls short, since it allows detection of lightweight elements. In EFTEM analysis an electron energy loss spectrometer is placed below the sample where in BF TEM the screen or camera would be. Electrons are sent through the sample. If an electron hits an heavier atom it loses more energy than were it to hit a lighter atom. Reference data about the energy loss from these collisions is available per atomic element, so a spectrum can be calculated. The energy loss information can be used for a single spot, giving a spectrum of the material at that spot, or the beam can be filtered for only one energy level (i.e. for one element), to map at which spots in the sample this element is present, this technique is called EELS (electron energy loss spectroscopy). Optionally, different maps can be overlaid afterwards to view multiple elements at once. EFTEM is not a full replacement for EDX, because detection of heavier elements is limited.

3

Failure mechanisms in thin amorphous silicon electrodes

Literature research proved that amorphous silicon thin films are promising electrode materials (see section 2.3.3). In this experiment the failure mechanisms in these lithium-a−Si thin film batteries are researched using microscopy and spectroscopy. A sample was prepared using magnetron sputtering 220 nm of silicon is deposited on copper foil substrate. After cycling the samples were observed using TEM and SEM.

3.1. Experimental

220 nm amorphous silicon is deposited on Cu foil to serve as current collector (the copper) and electrode (silicon). The copper foil is cleaned with aceton first, and then placed in the sputtering chamber. A two minute argon plasma pre-sputtering treatment was used to clean the foil of any impurities on the top layer, such as CuO. The magnetron sputtering process was then started at a deposition rate of 1.1 Å of silicon per second. Argon gas base pressure was set at 1×10^{-7} mbar with a gas flow rate of 20 sccm.[i] Before the actual sputtering begins, the silicon source is cleaned in the pre-sputtering step.

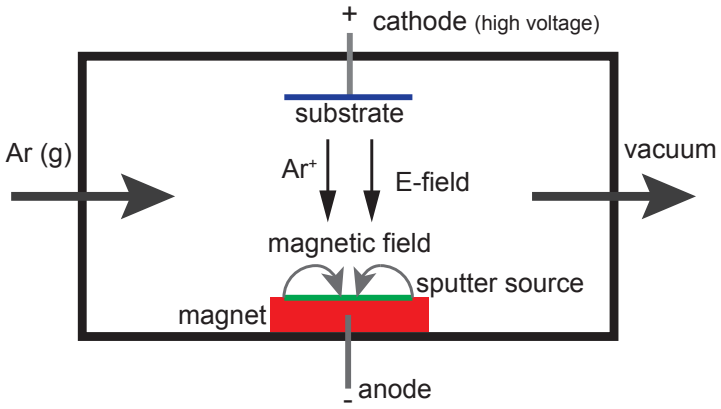

Figure 3.1: Schematic view of a magnetron sputtering machine. Argon gas is inserted in a high vacuum chamber. The source is placed on a solenoid magnet which creates a magnetic field as indicated. At the top a high voltage is applied in the meantime, generating a strong electric field. The electric field ionizes the argon, and the ions will now interact with the magnetic field. Due to the Lorentz force the ions will spiral towards the source material and sputter some of it away. Some of this sputtered material will then end up on the substrate in a uniform layer.
Pre-sputtering is done using the same principle as sputtering. Here too, a layer of material is removed from the source, but a shield is placed between the substrate and the source, to prevent the impurities that are sputtered away to be deposited on the substrate.

[i] For detailed parameters, see appendix A.1

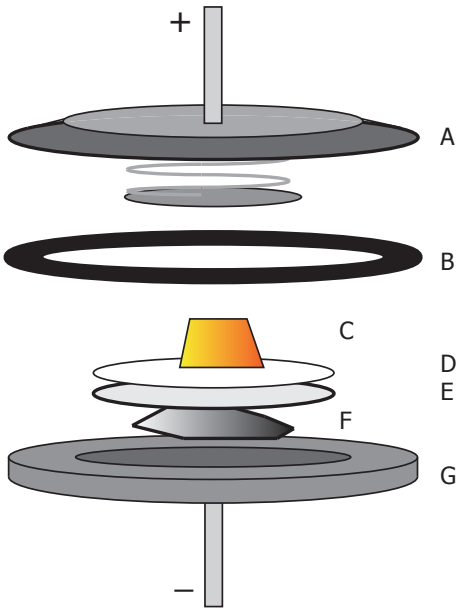

Figure 3.2: Diagram showing the components of the battery assembly.
A: top holder, **B**: rubber ring (insulates the top and bottom part), **C**: Copper foil with carbon coated side down, **D**: thick filter (separator sheet), **E**: thin filter (separator sheet), **F**: lithium, **G**: bottom holder.

About 0.5 cm² measuring samples were cut from the foil and assembled in a battery holder (see figure 3.2) in an argon filled glovebox. The weight of the silicon available can thus be (roughly) estimated to be 26 µg (using $\rho_{Si} = 2.3290$ g/cm³). The electrolyte (EC-DMC 1M $LiPF_6$) is added in soaked separator sheets. A spring presses together the components to ensure good conductive contact between them. The experimental battery uses a pure lithium metal anode, making the silicon the cathode in this case, since it has has a lower potential than lithium metal. Lithium is used because it is the reference material in lithium-ion batteries. This will also simplify the spectroscopy with only lithium and silicon as active battery components.

As seen in 3.2, two separator sheets are used. The thick sheet hold the electrolyte, since it can hold fluid. The thin sheet does not hold any fluid, but it is there to protect the thin silicon surface from damage by the rough thick sheet.

Charging and discharging was done using a galvanostat (Autolab PGSTAT302N) to a cut off voltage of 3 V and 0 V respectively. Because it has been reported that fully discharging a Li-Si battery is a big influence on capacity loss (see 2.3.3), a second set of samples was cycled between 3 V and 0.2 V. The 0.2 V was chosen based on the discharge curves found when performing full discharges. Samples were cycled a number of times to either a lithiated or a delithiated state. The lithiated state is expected to give more information about the swelling volume and properties than the more delithiated state will give, since the latter will show a rougher silicon surface. After cycling the cell, it was disassembled in a glovebox. The samples were washed in DMC (electrolyte without salt) to clean of the $LiPF_6$ salt present in the electrolyte (as done by Obrovac and Christensen [47]). Once the samples finished drying, the surface was imaged using SEM (Hitachi S-4800 and JEOL JSM 6500F) and EDX spectroscopy was performed.

3.1.1. Sample preparation for TEM

Using a Ga source focused ion beam (FIB) (FEI Strata DB235), a lamella measuring 10 by 6 µm is be cut from the sample, to allow for TEM observation.

First cross shaped markers are milled at 330 pA current to aid the script that will mill the lamella. Before sputtering away the area around the desired TEM sample, 1 µm of Pt is sputtered on the sample area, preventing damage to the surface of this area by ions used in milling. Then, the area on the sides and underneath of the sample is milled away at a 5.5 µA current. To free the section, the sides are removed, but leaving a small piece attached. Finally, this last piece will be removed as well. Doing the

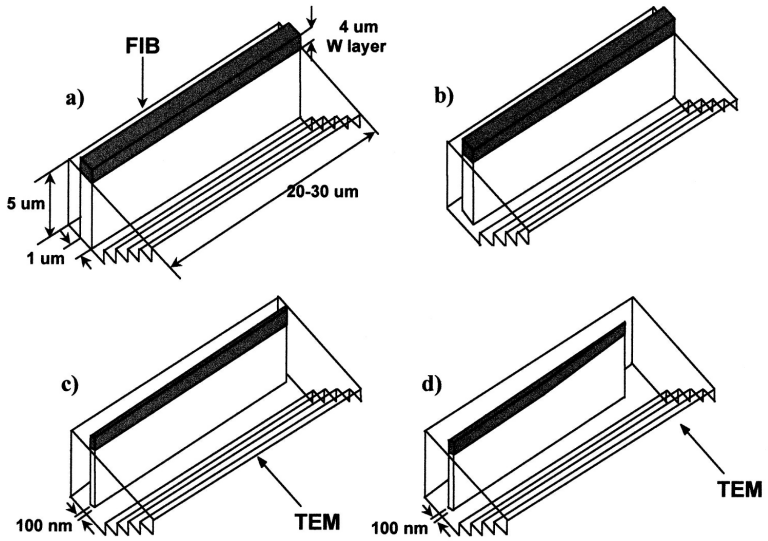

Figure 3.3: Schematic diagram showing how the FIB lamella preparation is done. (Source: Giannuzzi and Stevie [53])
a) The Pt has been deposited and the sides of the sample are freed. **b)** The bottom of the sample section is freed. **c)** The sample is thinned. **d)** The sample is milled under an angle to make one side extremely thin (optional).

last cut in a seperate step minimizes vibration of the sample, which could top it over which and make it impossible to take out. The removal of the sample is done under a microscope by using a glass patch pipette. Lamella are directly transferred to a chip, to be placed on a SiN window. The lamella were characterized and quantitatively analysed using bright field TEM, STEM, EELS mapping and EDX on a FEI Tecnai G2. EDX mapping and additional STEM imaging was done on a FEI Titan G2.

3.2. Results

Voltage-time curves from the galvanostat are analyzed and properties for the sample cells are calculated in this section. Results from the quantitative analysis are presented and described. Some calculations are presented to match quantitative results with qualitative results.

3.2.1. 0 V lower cut off voltage

Discharging one sample to 0 V resulted in the discharge curve shown in figure 3.4. After disassembling the battery in the glovebox, the silicon layer on the sample seemed half opaque, showing the copper underneath when viewed under an optical microscope at 1000× magnification. Some silicon was visibly detached and present on the separator sheet as can be seen on figure 3.6. Using a new sample in

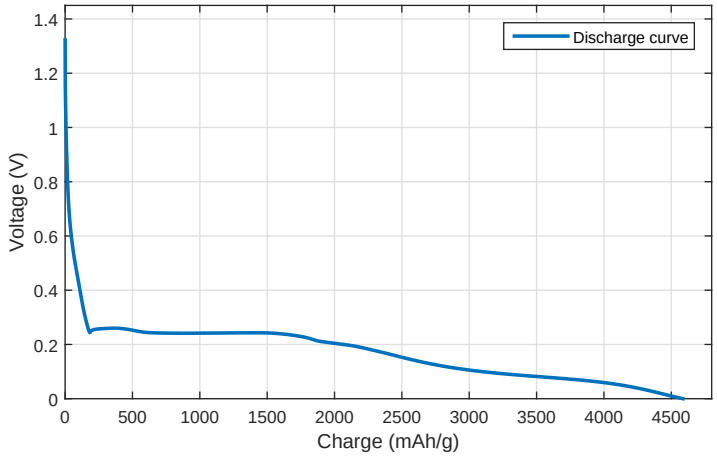

Figure 3.4: Discharge plot for the one discharge at 100 µA of silicon on copper foil in a coin cell set up. Notice the plateau around 0.2 V.

the same experimental setup, multiple charge-discharge cycles were performed at a charge/discharge rate of $\pm$100 µA. Upon opening the cell, it was visible that almost all the silicon had come off of the copper foil and large particles of silicon were clearly visible in the electrolyte. As seen in figure 3.5, the apparent capacity of the battery is halved after every cycle for the first two cycles, which can be fit to an exponential curve. For the last two discharges the capacity does not seem to decrease much further.

SEM analysis was subsequently performed to examine the micro-structure of the samples. Figure 3.7a clearly shows detached flakes of material on the copper foil substrate. From EDX analysis (figure 3.8) it was confirmed that the flakes still present on the copper did not contain any heavy elements other than silicon and some oxide and that the substrate is pure copper, which means total detachment of silicon on these areas. The detected oxygen could have been inserted in the sample during battery operation or during exposure to air (while transferring the sample from glovebox to the SEM device). The flakes are estimated to be around 2.5 µm thick (figure 3.7b), which is over 10 times more than the original thickness of the silicon layer.

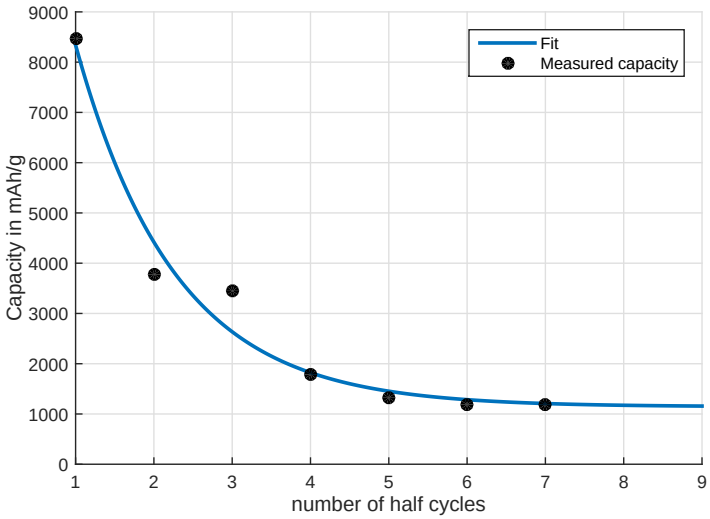

Figure 3.5: Plot of the capacity for a sample cycled multiple times. A fitting line was calculated using MATLAB for the equation $Q = a \cdot e^{-b(x-1)}$ with parameters $a = 7196$, $b = 0.7869$ and $c = 1144$. The raw discharge data is attached in the appendix, figure A.1.

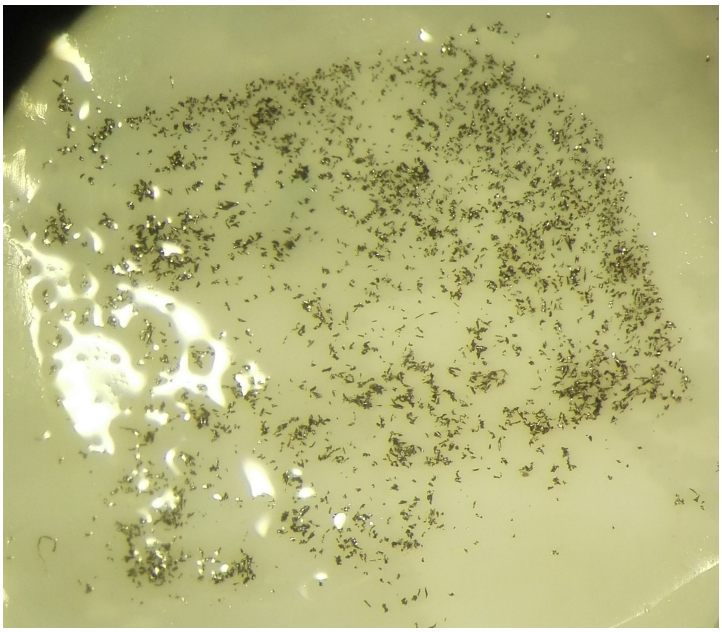

Figure 3.6: View of the separator sheet, corresponding to the capacity graph of 3.5, showing large flakes that detached from the copper foil

a. 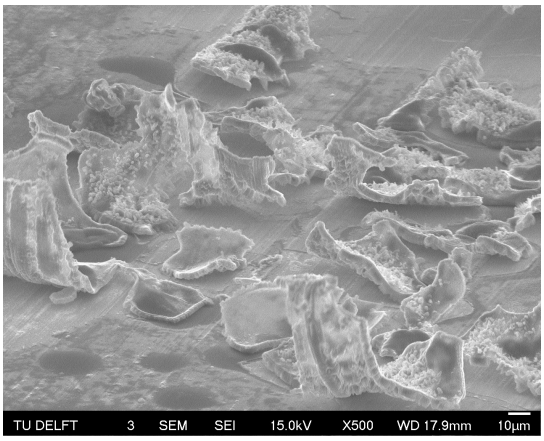

b. 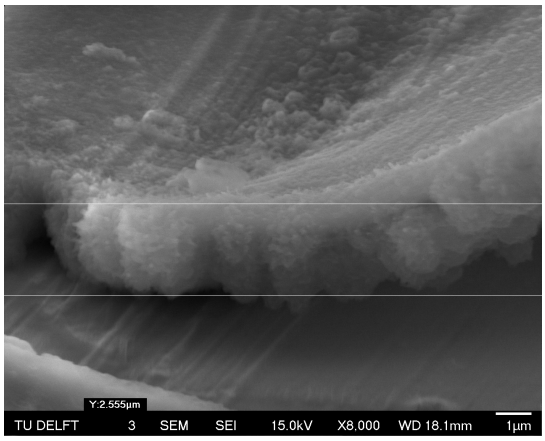

Figure 3.7: SEM images characterizing the surface showing large flakes. b: An estimation of the thickness was made of 10 µm. Since the silicon layer deposited had a thickness of 220 nm, this would imply that the top layer went through a volume change of more than 10 times.

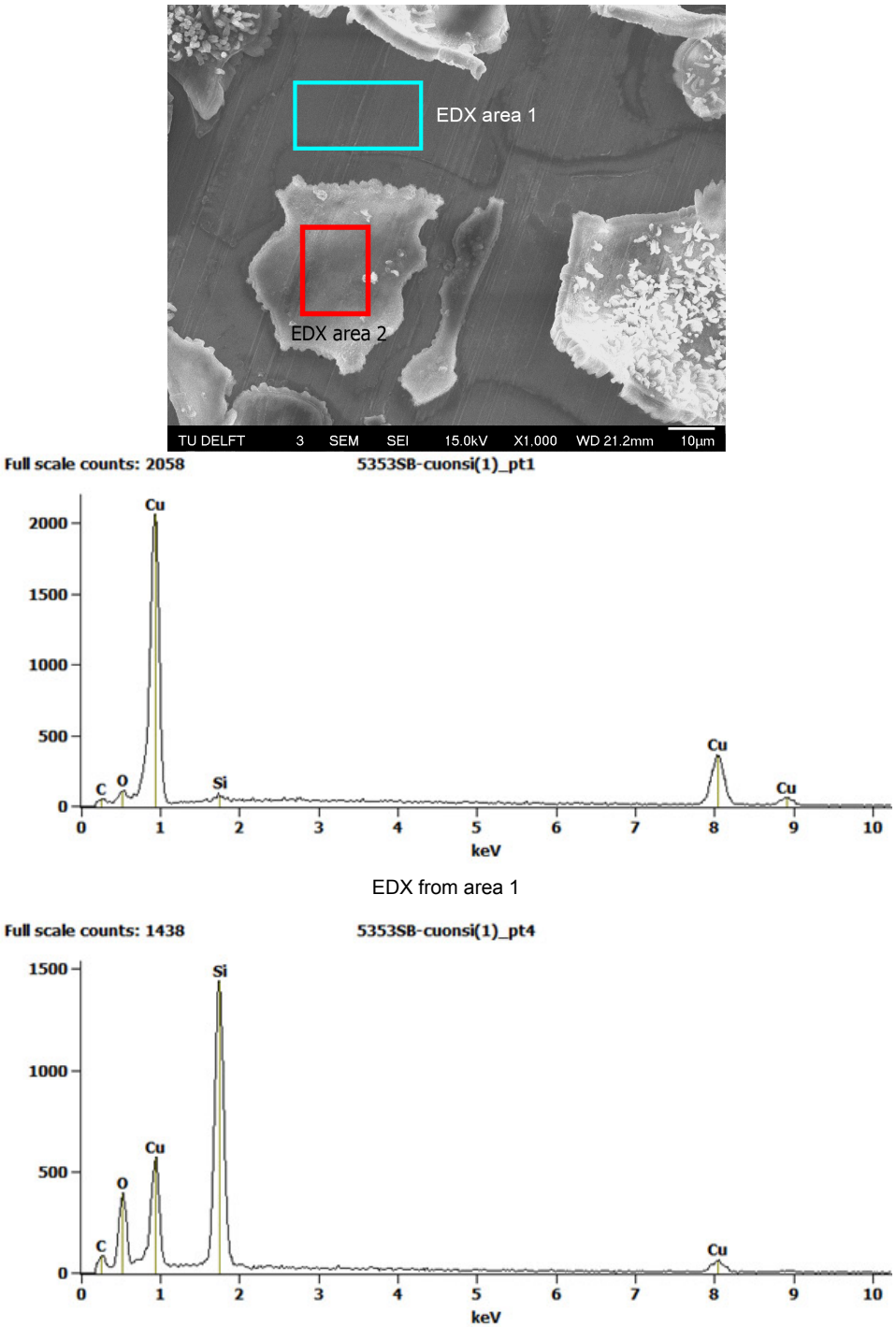

Figure 3.8: Top: SEM image of the sample showing two swollen pieces of silicon on top of the copper foil substrate Middle and bottom: EDX analyses from the marked areas, showing that the shilver mainly consists of silicon. Because this sample was exposed to air for some time, the oxygen is most likely due to some SiO_2 formation.

To confirm the severe detachment of silicon, the experiment was repeated for 5 cycles (figure 3.9). However, this resulted in much better cycle life And the severe swelling and current collector detachment could not be replicated any subsequent tests.

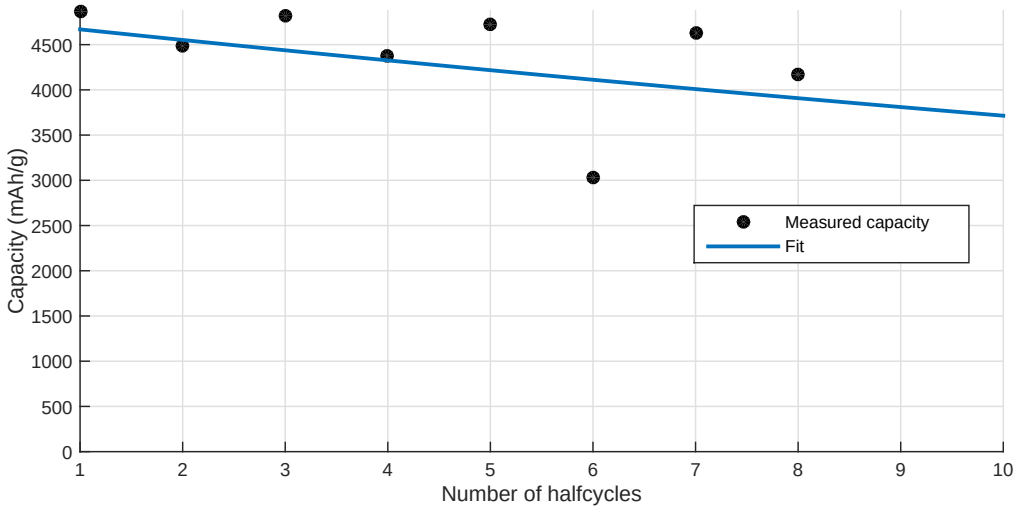

Figure 3.9: A second sample cycled between 3 V and 0 V demonstrated much better cycle life. The fit line uses equation $Q = a \cdot e^{-b(x-1)}$ with $a = 4789$ and $b = 0.02541$. This fit predicts 50% capacity loss after 28 half cycles or 14 full charge/discharge cycles.

3.2.2. 0.2 V cutoff voltage

All the cycles were repeated for a lower cutoff voltage of 0.2 V. This in an attempt to avoid irreversible lithiation and crystallization as explained in the theory. The value of 0.2 V was chosen based on the discharge plots to 0 V, the plateau for the tested cell set up was visible there around 0.2 V instead of at 50 mV. The exact voltage at which the phase change occurs depends on the battery resistance and electrolyte, which explains this difference.

One sample was discharged once to 0.2 V (figure 3.10) and another sample was cycled 5 times to a lithiated state. The cycle life behaviour over 5 cycles was similar to that observed in the sample from figure 3.5, but the silicon had not detached enough to be visible using optical microscopy. In fact, no clear difference was visible between the cycled sample and pristine pieces of silicon on copper foil when viewed with an optical microscope.

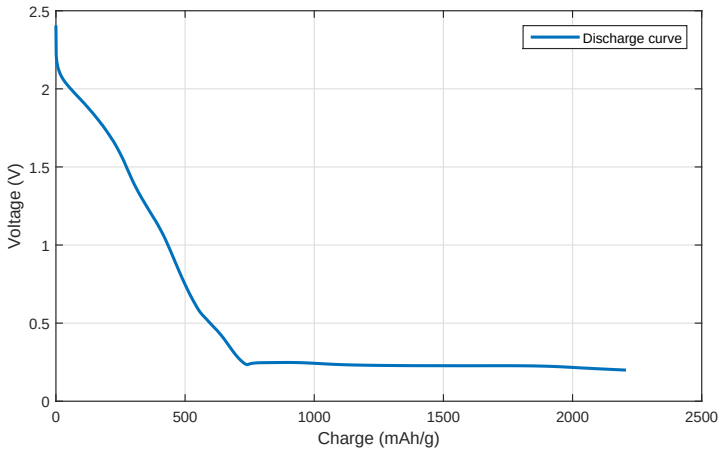

Figure 3.10: Discharge plot for one discharge to 0.2 V. Notice that the theoretical capacity of 4200 mAh/g is not reached contrary to the other samples (see 3.4). This indicates that the sample is most likely not fully lithiated.

3.2.3. SEM images

To compare the structure of the silicon electrode at various discharge points, SEM images were taken of several samples as shown in figure 3.11. Cycling the silicon clearly roughens the surface, and detached particles, this can be seen in figure 3.11c and 3.11d. This is a cause of capacity loss.

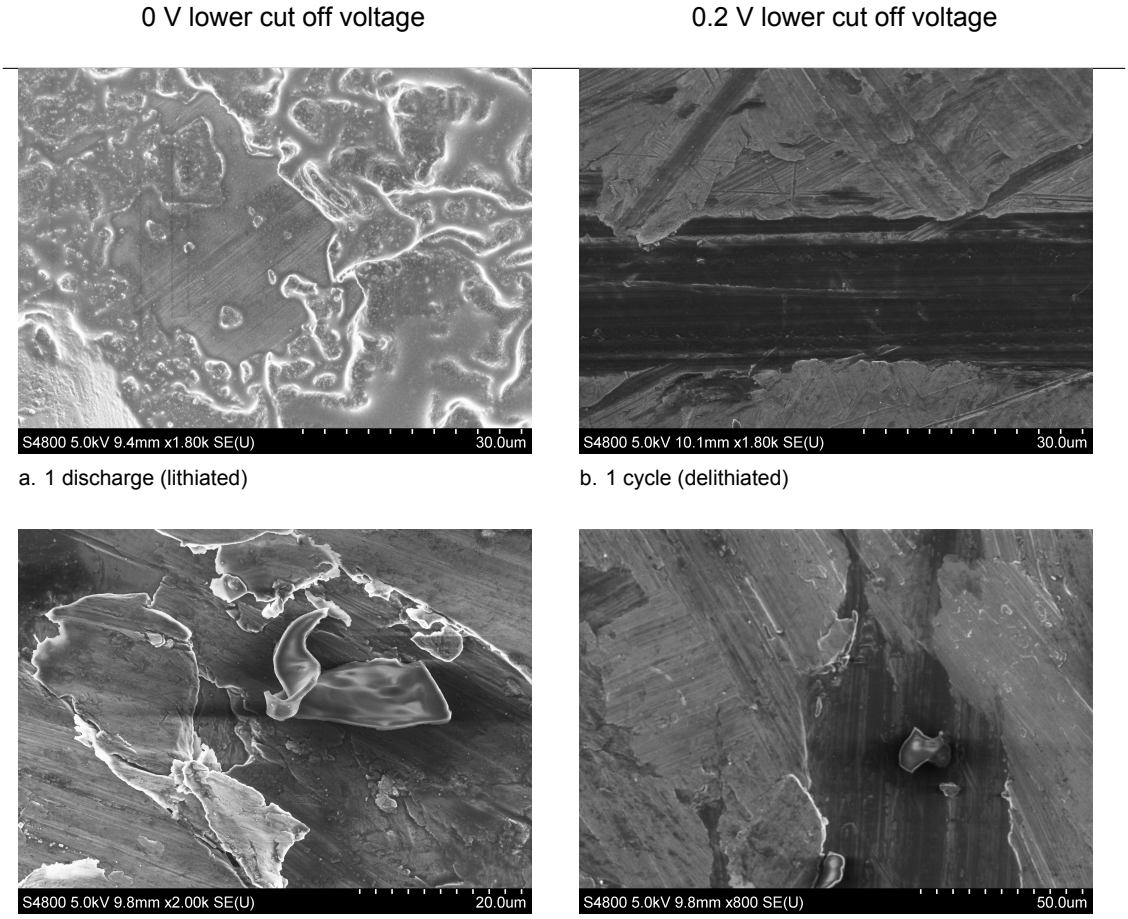

a. 1 discharge (lithiated)

b. 1 cycle (delithiated)

c. 5 cycles (lithiated)

d. 5 cycles (lithiated)

Figure 3.11: Comparison of the surface as observed using SEM at 2000× magnification. The samples c and d, that went through 5 cycles have a clearly more detached surface than the samples which were discharged once (a,b). Sample a., which was only discharged once and not charged, shows a less rough surface than the other three samples.

3.2.4. Lamella analysis

A lamella was taken from a sample discharged once (lithiated state) to 0.2 V (figure 3.10). This sample was chosen for the best chance of success of creating the lamella, based on the SEM images of the other samples.

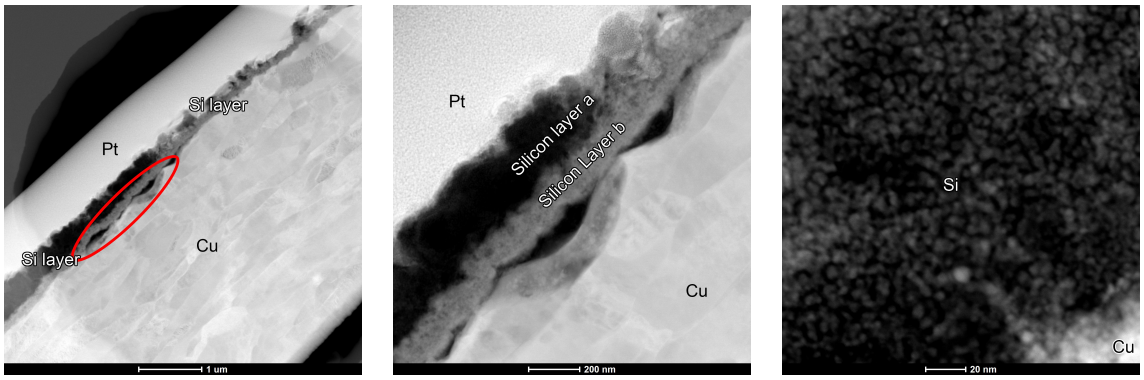

a. b. c.

Figure 3.12: a. Low magnification STEM image of the lamella showing that silicon detached from the copper current collector (see red marker) and that the silicon layer is split in two layers with different properties.
b. Medium magnification STEM image covering the full height of the silicon layer. It is very clear that the silicon layer has changed into two layers with different properties.
c. High magnification STEM image of the lamella, showing a detail of *silicon layer b* in view. A structure particles in with voids between them is visible. This is typical for amorphous silicon in general.

From 3.14 multiple important features can be described. Firstly, silicon layer has detached from the copper foil over most of its area (figure 3.14a), as was also observed on the SEM images in figure 3.7 and 3.11. Secondly, from the thickness mapping (figure 3.14b) the silicon layer is clearly divided in two regions (labeled *a* and *b* in figure 3.12b), with the layer that faced the electrolyte in the battery (platinum side) having the lowest density (assuming constant lamella thickness), indicating the presence of lightweight material such as lithium. EFTEM mapping (figure 3.14b,c) shows that the top silicon layer (*layer a*) is lithium rich, with the bottom silicon layer being mostly absent of lithium. It is therefore likely that only the top layer is lithiated. The total thickness of the silicon is about 300 nm, with a ratio of about 2:1 between layer a and layer b. Assuming that *layer b* (100 nm), the silicon layer not containing any silicon, did not swell, then the swelling of *layer a* (200 nm) is $\frac{200\text{nm}}{120\text{nm}}$, or 67% swelling. This is close to the 60% swelling for the LiSi state.[26] Again, making the assumption that only the LiSi state is present, a rough estimation of the capacity can be made using equation 2.7 and the silicon weight (26 µg). The capacity is then estimated to be 25 Ah, using a specific capacity of 957 mAh/g.

Oxygen is detected throughout the sample, with some overlap between lithium and oxygen (white colour in figure 3.14e). High magnification STEM (figure 3.12) of the bottom silicon layer (*layer b*) shows numerous voids in this silicon layer. The diffraction pattern of a spot in the top layer of lithiated silicon (figure 3.13) shows that most of this layer is amorphous with some smaller crystals present (bright spots).

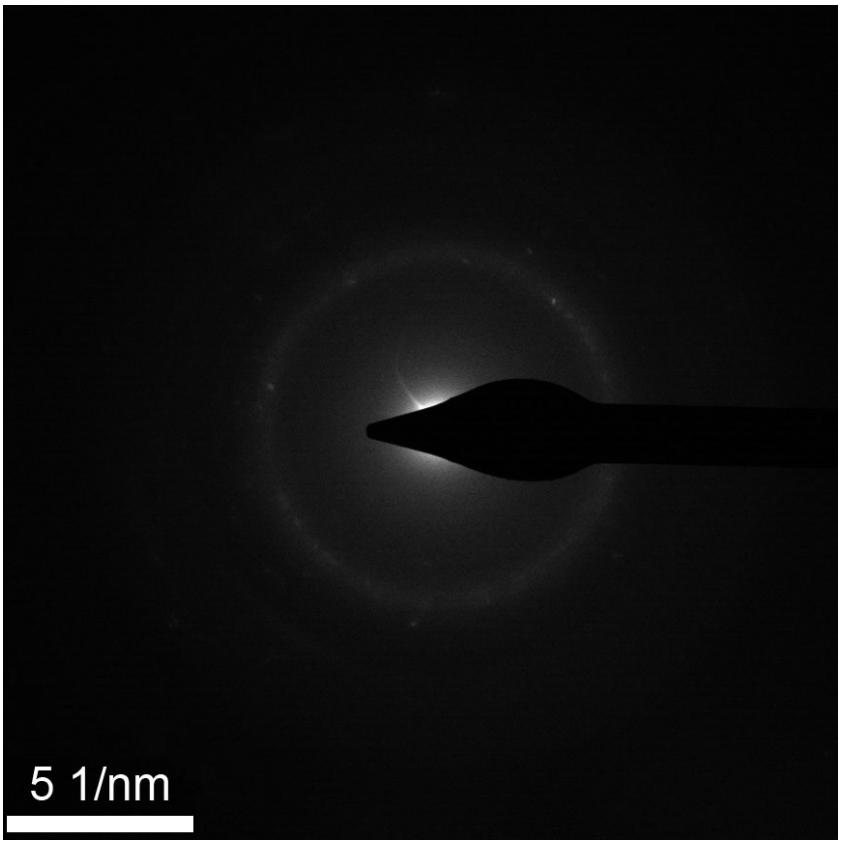

Figure 3.13: Diffraction pattern for a spot in the top lithiated silicon layer. Few bright spots are visible, showing that this layer is mostly amorphous.

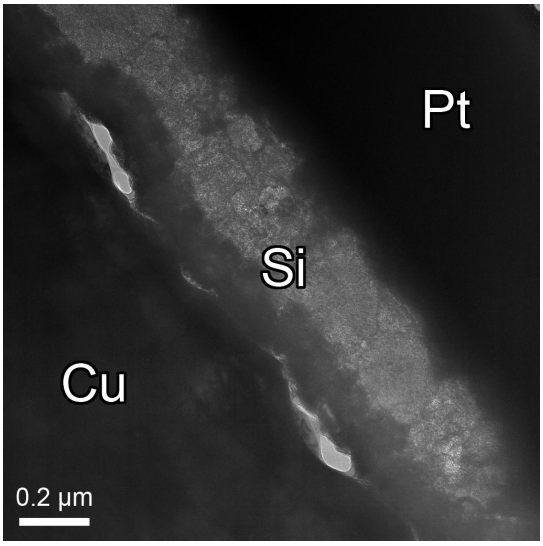

a. Bright field TEM of the silicon layer

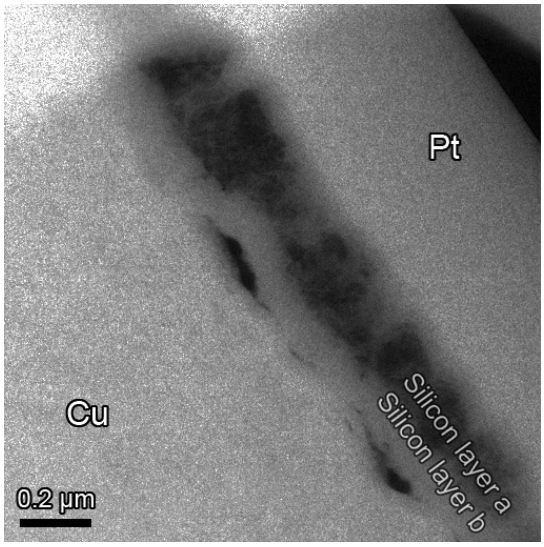

b. Thickness map of this area (lighter is thicker)

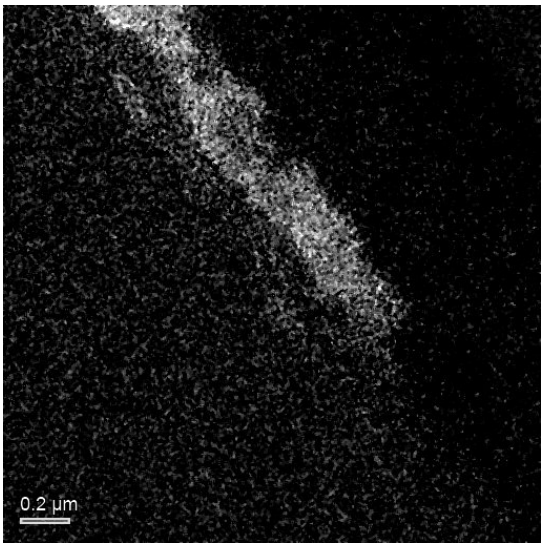

c. EFTEM map of the lithium intensity for the same area as in b.

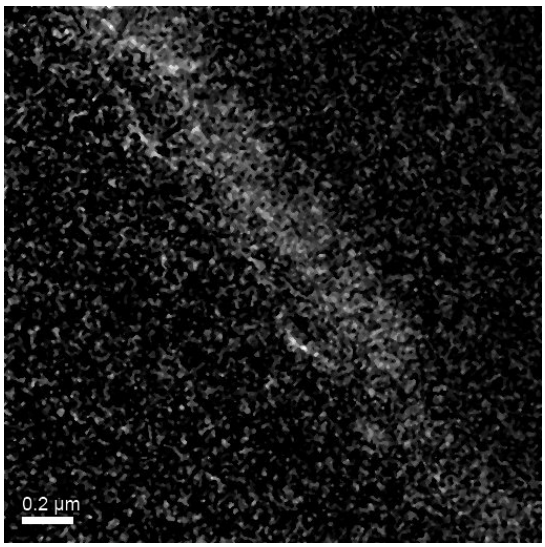

d. EFTEM map of the oxygen intensity for the same area as in b.

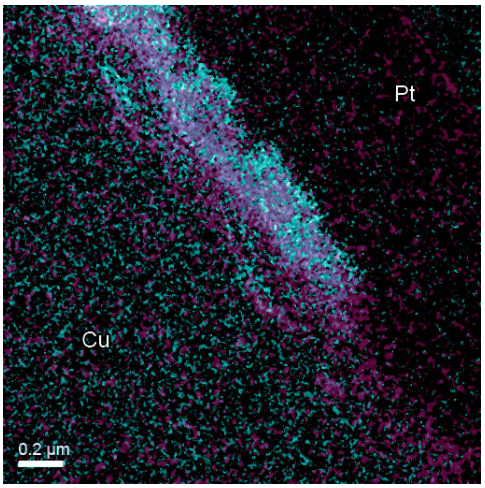

e. False colour overlay for the lithium (blue) and oxygen (red) map

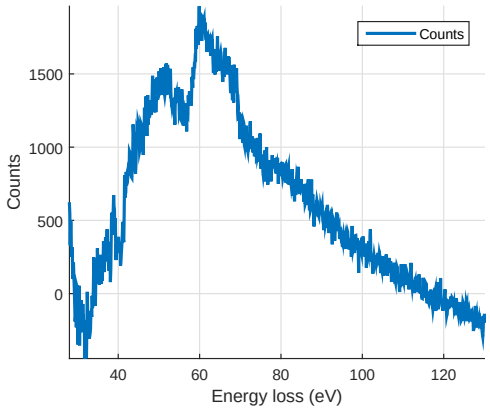

f. EELS spectrum showing that lithium and lithium compounds are detected around 55 eV, the background detections can be found in the appendix (figure A.3). No silicon edges were detected (99 eV).

Figure 3.14: Various analysis results from the silicon layer area of a sample discharged once to a lower cut off voltage of 0.2 V.

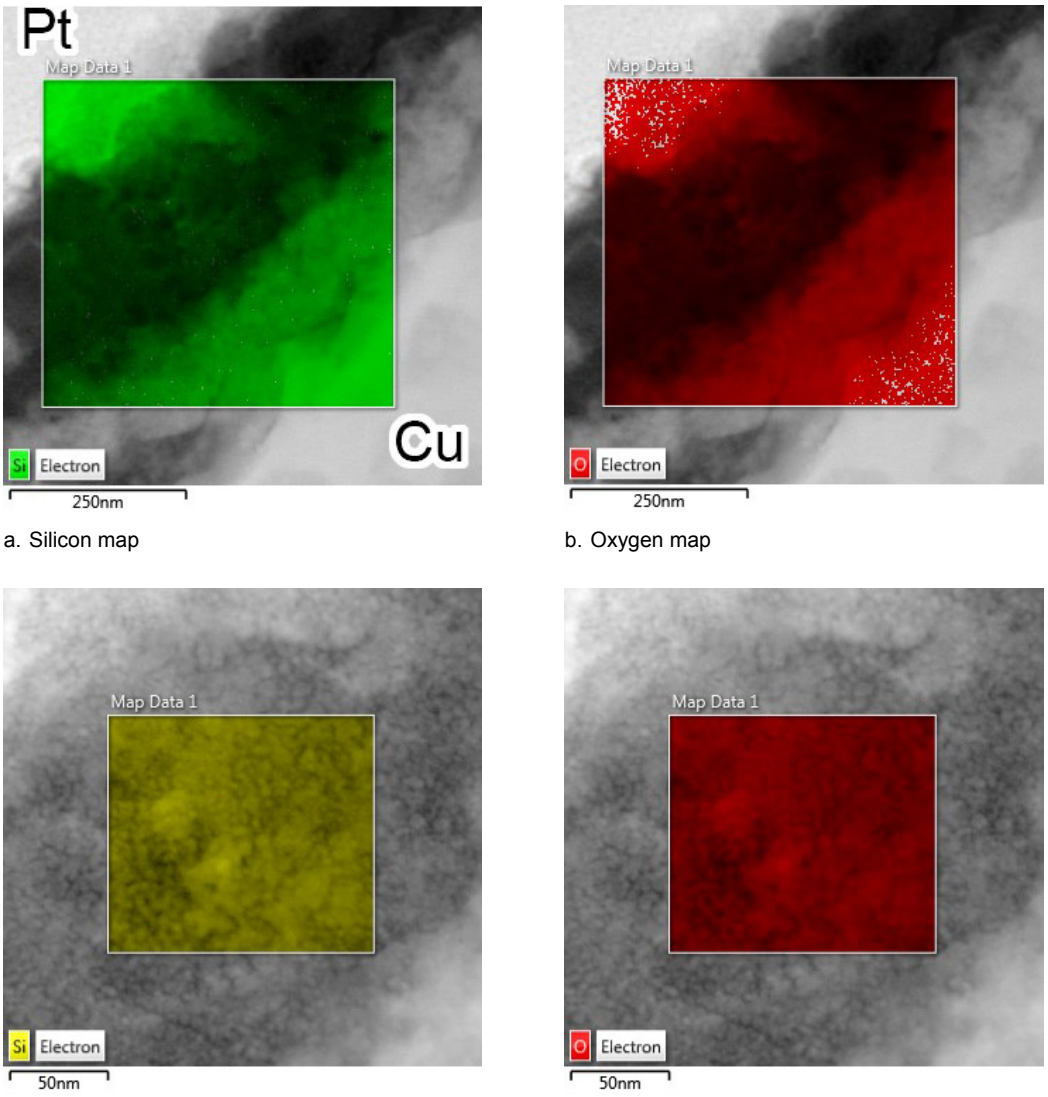

a. Silicon map

b. Oxygen map

c. Silicon map

d. Oxygen map

Figure 3.15: EDX mapping for silicon and oxygen. The top two maps are for the entire silicon area, showing most oxygen present in the thin, unlithiated part of the silicon and the silicon layer b (copper side) containing more silicon than layer a. The bottom two maps are captured in layer b, showing that the layer is porous with voids between the particles. For supplementary data see appendix A.4.

3.3. Conclusion and discussion

The flat plateau for the first discharge as seen in figure 3.4 was also observed by Jung *et al.*[45] and means that multiple lithiation phases exist in equilibrium, this equilibrium only occurs for the first cycle, which is as expected from literature. Some of calculated specific capacities were higher than the theoretical capacity of 4200 mAh/g for silicon, this is due to the uncertainties of the estimated silicon weight, cell and wire resistance and side reactions occurring.

One of the samples showed much more swelling (10 times) than known from literature (320%). Based on the apparent fluffy structure of the flakes as seen on SEM images and lack of traces of heavy materials other than silicon found in the flakes, it can be assumed that these flakes consist of silicon, lithium and void space. The swelling of 10 times could not be repeated with any of the other samples. But, during the experiments the electrolyte solution ran out and even though fresh electrolyte of the same specifications was obtained, it was still suspected however that this change in electrolyte was a possible cause of this unrepeatable large swelling. Therefore some of the fresh electrolyte was deliberately exposed to atmospheric air for 24 hours to simulate (older) decomposed electrolyte stored outside a glovebox and to allow moisture and oxygen to react with the electrolyte. This should result in HF formation,[54] although HF does not react with pure (unoxidized) copper or silicon. Cycling with this decomposed electrolyte could also not repeat the large swelling.

The current collector detachment, as seen in SEM images (figure 3.11), is the most likely reason for the reduced capacity of the silicon film. The fact that the capacity does not decrease much more after the first two cycles might indicate that current collector detachment was mainly occuring during these first two cycles. The exponentially dropping capacity is similar to the behaviour observed in literature of amorphous silicon thin films on metal foil.[13 55] The capacity loss in literature was significantly less than found in this experiment though. Bourderau *et al.*[13] hypothesised the capacity loss to be due to ”mechanical disintegration” and Obrovac and Krause[55] also explained the exponential capacity loss to be caused by silicon ”being disconnected during lithiation”, which matches the observations from this research.

Half of the samples were discharged to a 0.2 V lower cut off voltage. This should prevent a partially irreversible phase change from amorphous to crystalline lithiated silicon according to prior research, which would result in less stress in the silicon and better cycle life. SEM images confirmed that cycling to 0.2 V resulted in significantly reduced surface damage to the silicon layer. From TEM, EDX and EFTEM observation (figure 3.14) it is found that not the entire silicon layer is lithiated after one discharge to 0.2 V, but a 100 nm layer of mostly pure silicon remains on the current collector side. This layer is detached from it though, which implies that stress from swelling of the top layer was transmitted to the bottom layer. It cannot be ruled out that the platinum applied during lamella preparation contributed to the detachment. Furthermore, EDX mapping showed high silicon intensities not just in the silicon layer, but in the platinum and copper layer too. This is subject to further research. If silicon is really present in large quantities throughout the platinum and copper, this would indicate problems in the sample preparation process. Another possibility is that the EDX mapping data was not processed correctly for presentation.

The layer identified as containing lithium (lithiated) using EFTEM, showed a volume change of 67% and only few crystalline features were identified in its diffraction pattern. This result corresponds to the lithiated state of silicon (LiSi), which reportedly swells 60%[26]. However, this percentage is relative to crystalline silicon instead of amorphous silicon. The accurate swelling percentage will have to be established by measuring a pristine lamella for comparison. The few crystalline features detected may be SiO_2 crystals or the crystalline lithiated phase $Li_{4.4}Si$. It is unlikely that the latter is present given the low swelling percentage and low capacity found in the sample. The lack of any clear overlap between lithiated silicon and oxygen makes makes it unlikely that the oxygen was embedded in the sample during battery operation. However, the sample was exposed to air for more than two days, where some SiO_2 must have formed on the silicon surface.

Observing a lamella from a sample discharged to 0 V and from a pristine sample was not possible during the time of the research, but would be recommended to see the lithiated fraction in that case. However it is expected that the silicon detachment will be much worse. This might result in total silicon detachment during lamella preparation.

4

Observing the SEI layer on crystalline silicon

In order to observe the SEI layer, crystalline silicon discs were ion polished to allow TEM observation. Due to unknown reasons, contaminations were detected on these samples that prevented any solid conclusions about the SEI layer. It was not possible in the available time for this research to find the source of these contaminations, instead, a different experiment will be suggested in this chapter. This experiment is a quasi in situ set up that would allow direct observation of the SEI layer. Its thickness, density and composition can all be studied using TEM and EDX.

4.1. Ion polished silicon discs

In this experiment it was attempted to observe SEI layer formed on ion milled crystalline silicon discs using TEM and EDX.

4.1.1. Experimental

Starting with a piece of silicon wafer, 3 mm diameter discs are cut and polished to a thickness of 60 µm. The thin discs are placed in an ion polishing machine were a hole is milled in the centre of the discs. At the edges of the hole, the silicon is thin enough to be observed using TEM. The 3 mm discs fit in a standard TEM cartridge which can be placed in a TEM holder. Inside a glovebox, the sample is placed in a TEM cartridge, a wire is connected to the metal cartridge and a galvanostat, and the sample is placed inside a glass flask holding EC-DMC electrolyte. Lithium metal is connected to the other galvanostat lead and placed inside the flask too. The resulting liquid cell is then discharged once to lithiate the silicon. After discharging the sample was left to dry and TEM observation was done.

4.1.2. Results and discussion

From STEM images (see figure 4.3 and appendix A.5), a low density 'fluffy' layer can be seen at the silicon surface. Figure 4.3 seems to confirm that this is the SEI layer, since it mainly appears on the surface of the silicon. In figure 4.2 the difference between areas on the surface and the bulk silicon is clearer. However, this difference was also seen during TEM observation of a control sample, which hadn't been in contact with electrolyte. Similar EDX spectra as on the cycled sample were observed for edge and inner regions. This lead to the conclusion that the used sample preparation method is flawed, being unable to pinpoint the difference between contaminations and other flaws and a possible SEI layer. Therefore a more refined experimental set up is proposed.

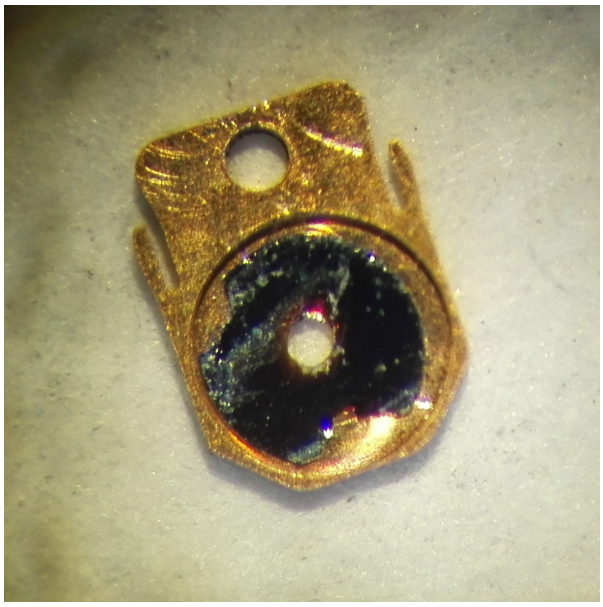

Figure 4.1: Sample placed in a TEM cartridge. The hole in the sample is made using ion polishing.

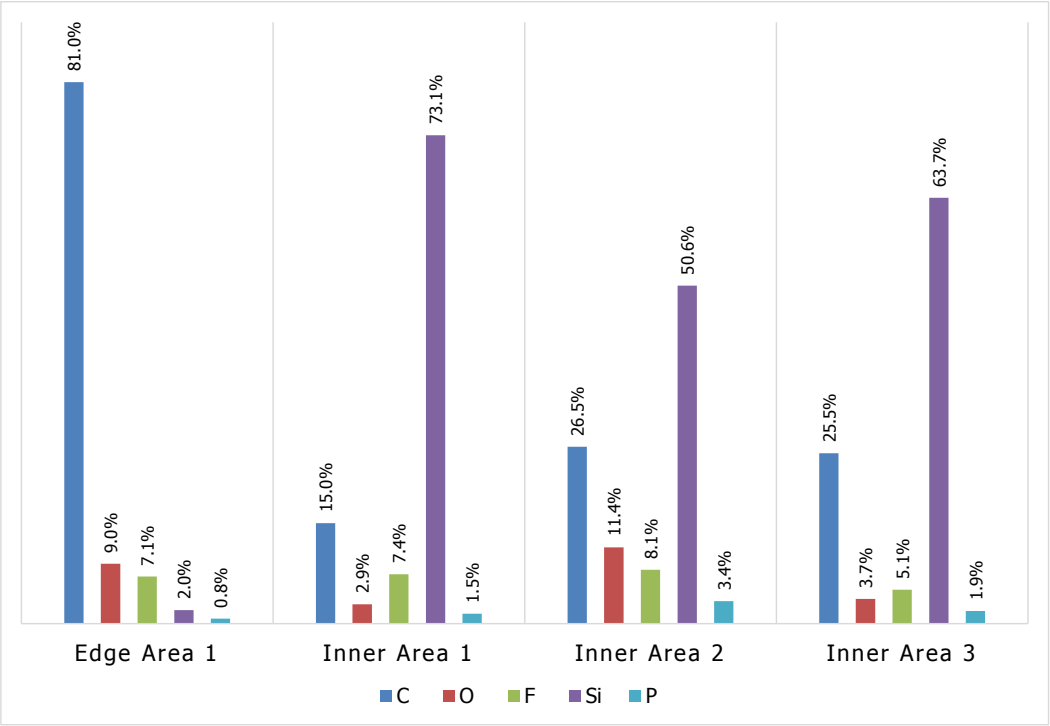

Figure 4.2: EDX analysis for four different areas of the sample, showing the atomic weight percentage for each area. The first area was located on the edge of the sample, the other three analysed areas were located several micrometers from the edge of the sample. For each area an average was taken of the spectrum for four individual points in the area. The graph shows that the difference in carbon content and silicon content differs significantly between the edge area and the areas located away from any edge.

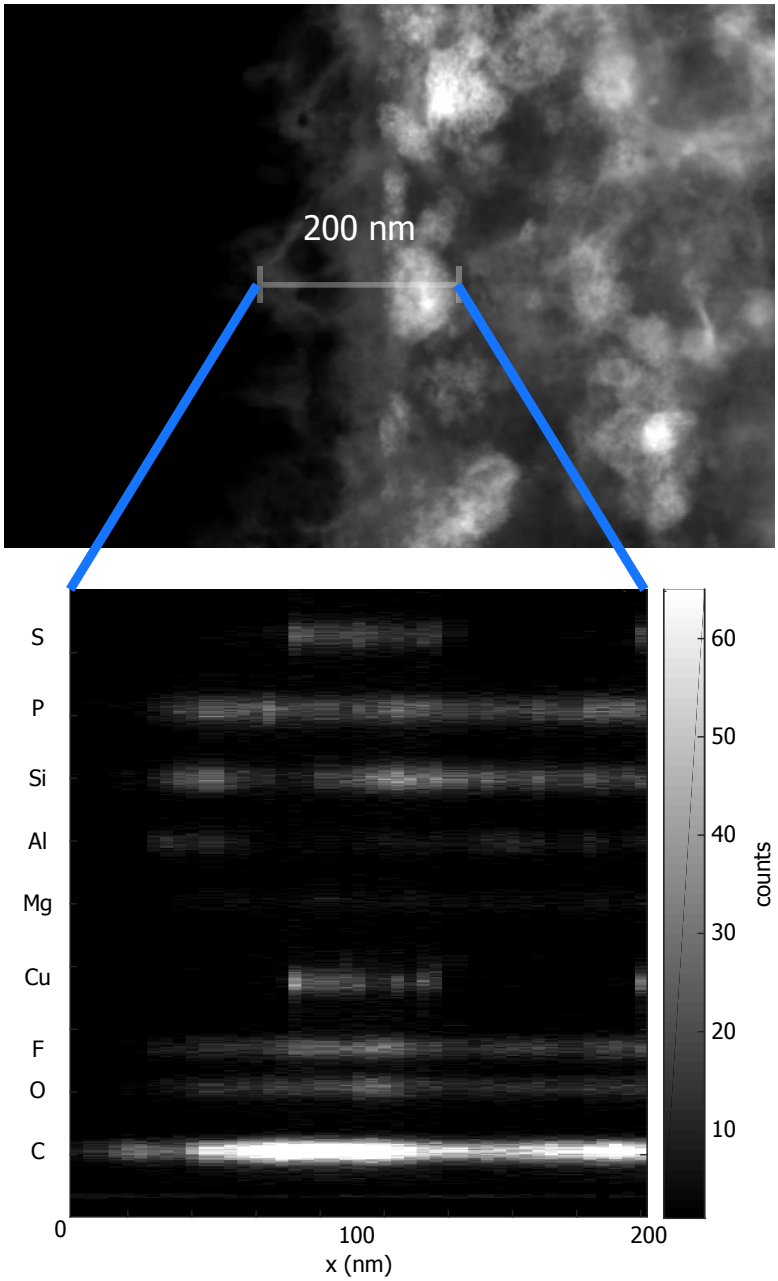

Figure 4.3: EDX profile of the edge of a discharged sample. The top part of the image (STEM micrograph) shows the line where the profile was captured. The lower part of the image shows the number of counts for each found element for corresponding points along the profile.

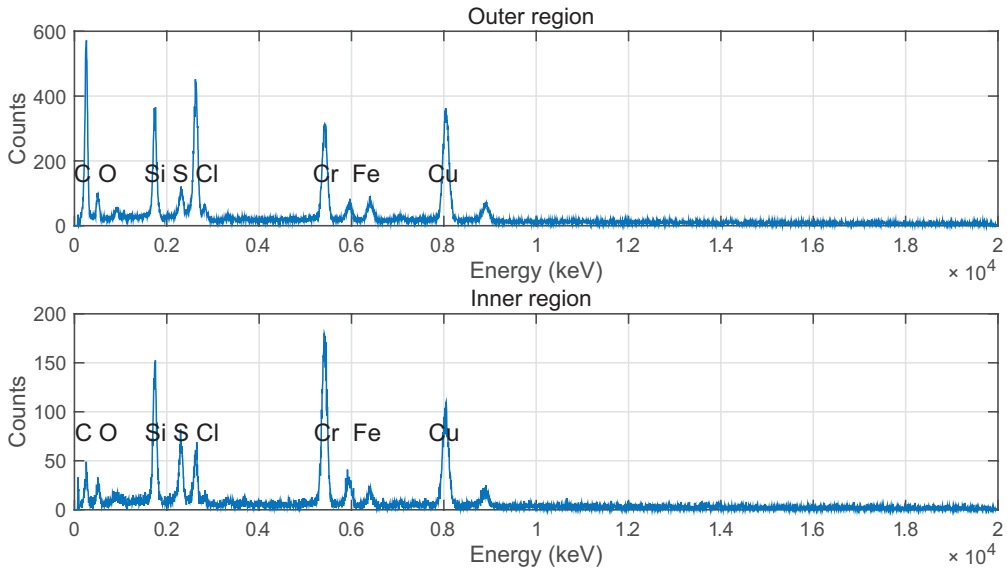

Figure 4.4: EDX analysis of the inner and outer (edge) regions of a sample that hasn't been in contact with electrolyte. The carbon content differs a lot between the edge regions and the inner region similar to what can be seen for a discharged sample in figure 4.2.

4.2. SEI layer observation

The difficulties in observing the SEI layer are related to it's thinness, it's reactivity with air and moisture and it atomic similarity to common organic compounds (high carbon content). Therefore, to successfully observe it, a sample should have fine details (for visibility of thin parts), should be well shielded from atmospheric air and should be prepared with minimal contact with organic material, in a clean environment.

The best solution fitting these criteria is a semiconductor structure. Preparation of semiconductor chips is done in a cleanroom environment and strong acids are used during the process, removing all organic material. Sub-micrometer structures can relatively easily be created from silicon wafer material.

The silicon chip is not just the substrate or sample holder, but should part of it should function as active silicon electrode material too. To observe thin structures, the electrode is also required to be very thin, but a rigid substrate is needed. For this, a special type of wafer is used, called silicon on insulator (SIO). This wafer structure consists of a relatively thick silicon substrate layer, on top of that a thin layer of (electrically isolating) SiO_2, with a thin layer of silicon on top of that. The top layer of silicon is therefore insulated from the bottom layer. A so called window - an area thin enough to transmit electrons - is needed to observe the sample using TEM. To do this, a deep trench is etched from below up to the topmost silicon layer. This trench will only be a few micrometers wide, compared to the 300 µ thick silicon substrate. Etching these high depth-width ratios is called high anisotropic etching, and a technique called DRIE is most suitable for this.

Deep reactive ion etching, abbreviated as DRIE is an etching technique used to allow etching deep under the surface height of wafers (high aspect ratio). DRIE fits the gap between conventional etching (e.g. KOH) and mechanical processing of silicon.[56] The most used DRIE processes was first patented[57] and used by the Robert Bosch Gmbh company in the 1990s. This DRIE etching process is called the Bosch process. Trenches etched using this process are characterised by a sawtooth-like edges with a height of about 50 nm peak-to-peak when controlled well[58]. This is also the downside of the Bosch process, because a higher etching rate corresponds to a rougher edge.[59]

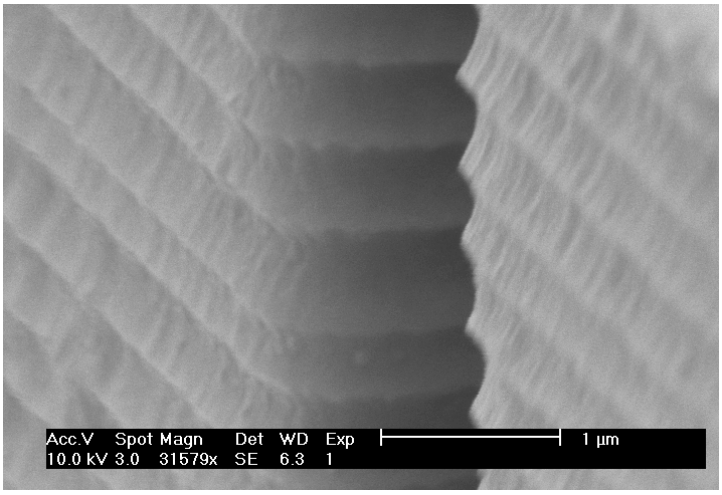

Figure 4.5: SEM image of the sidewalls of a structure made using the Bosch process. Source: Pgalajda, Wikimedia Commons [60]

The sawtooth edges are inherent to the pulsing principle behind the Bosch process. The main process uses two alternating steps, one being anisotropic plasma etching and the other being a polymerizing of the surface. During the etching material is removed, and during the polymerizing the exposed areas of the wafer are covered with a polymer layer which will protect these areas from the etching. An electric field is applied perpendicular to the wafer surface which will make ions in the plasma travel straight into the bottom of the trench, and keep only the bottom side free of polymers.[57]

4.3. Experimental

Starting with a 300 µm SOI wafer with a 200 nm SiO_2 layer and another 220 nm layer of Si on top of that, the first step in the preparation is to coat the bottom (thick Si) also with SiO_2. The top 150 nm

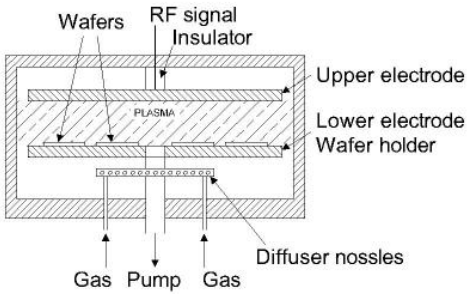

Figure 4.6: Illustration of a typical DRIE chamber showing the electrodes to generate the electric field and the plasma. Source: MEMSnet [61]

of the thin Si layer on top is converted to SiO_2 as well, leaving 70 nm of Si beneath it. Photoresist coating is applied to the bottom, and the pattern is written using e-beam lithography. After developing the photoresist, deep reactive-ion etching (DRIE) is used from the bottom, etching all the way through the thick silicon part of the wafer to form a window. Next the top SiO_2 layer is etched away and finally, a layer of Au is deposited on top of the thin Si layer, to act as a current collector. The process is illustrated and described in figure 4.7.

The finished chip is then transferred to a glovebox where the gold contact area is connected to a galvanostat. The chip is then submerged in electrolyte (EC-DMC 1M $LiPF_6$) and a lithium metal working electrode is placed in the electrolyte as well and connected to the other galvanostat wire. Cycling tests can then be executed, after which the chip is optionally washed in DMC and left to dry for at least 12 hours. The chip sample is inserted in a vacuum TEM holder and can be brought to the TEM outside the glovebox.

1. Section view of the starting material, a silicon on insulator wafer. Grey: Si, blue: SiO_2.

2. Part of the top layer of Si is oxidized to SiO_2 using thermal oxidation.

3. Part of the top layer of Si and a layer on the bottom are oxidized to SiO_2 using thermal oxidation.

4. Photoresist is applied and a window is etched in the bottom oxide layer using HF

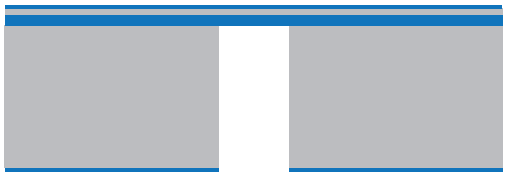

5. The thick silicon bulk material is now exposed. To make the window, deep reactive ion etching (DRIE) is used to etch it away perpendicular to the surface (Bosch process).

6. All exposed oxide layers are removed using HF etching.

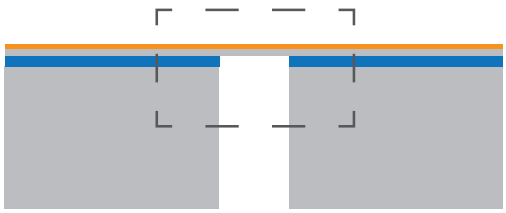

7. A thin layer of gold is deposited on the top Si layer. This will serve as the current collector.

8. (detail view) The chip is transferred to an ion milling machine (FIB) where a hole is milled in the window. The chip is now ready to be used.

Figure 4.7: Section view of the chip throughout the fabrication process.

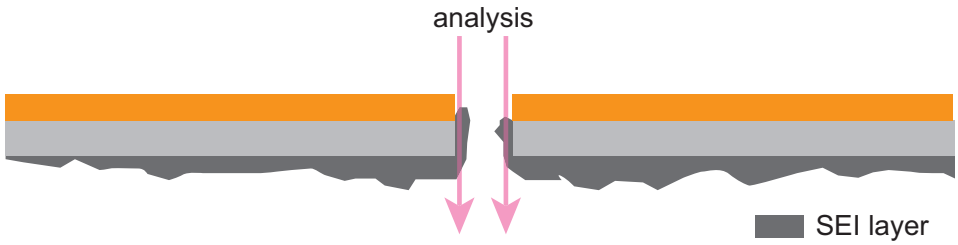

Figure 4.8: Detail section of the window explaining the reason for making the hole. SEI layer is expected to form over the entire silicon surface, but it's thickness, combined with the silicon and gold thickness will make TEM observation more difficult and influence EDX analyis results. However, on the sides of the window it should be possible to look directly through solely SEI layer.

4.4. Discussion

The advantage of using a chip windows instead of a cutting lamella from a macroscopic sample are reduced exposure to air and other contaminants. Since the SEI layer is very thin and reactive, reducing the steps needed in the process will increase the success rate for observations.

Executing the experiment fully in situ would give the most interesting observations, but TEM observation of experiments involving liquids (such as the electrolyte) is not ready for this type of experiment. Using solid electrolyte is also only in the experimental phase and this will likely result in no or different SEI layer forming.

The main disadvantage of using this type of chip for SEI formation is the usage of crystalline silicon. It is expected that most of the silicon around the hole will be amorphous due to the ion beam exposure during milling the hole, but how much crystalline silicon will be left is left to guess. It is possible that the crystalline silicon also fully lithiates and will detach from the current collector, making further cycling impossible.

5 Further research

Considering the possibilities and opportunities for Li-Si batteries, more experimental research will likely produce insightful results. In this chapter some interesting further research opportunities are presented and earlier research on these topics is reviewed.

5.1. Coated silicon electrodes

Yen *et al.*[62] found that coating the silicon electrode with a thin carbon layer will vastly improve cycle life. Capacity of the battery will be less than that of one using a bare silicon electrode though. Coating with other materials such as SiN might produce interesting results as well.

5.2. Predicting SEI layer growth

Even though the SEI layer growth is influenced by many parameters, Pinson and Bazant[28] managed to set up a simple model for SEI layer growth as a function of time. The model was tested against experimental results and proved to provide a good fit. This is not the only model, a more advanced model was developed and tested by Li *et al.*[31]. Applying the model to different types of electrodes would provide better hypotheses before performing experiments and would also be useful in commercial fabrication and application of lithium batteries.

5.3. Electrolyte additives

Adding additives to a standard electrolyte or replacing compounds in the electrolyte can influence SEI layer formation and thereby cycle life.

5.3.1. Inorganic additives

Since the SEI layer is a product of a reaction from the electrodes with organic components of the electrolyte, using an inorganic electrolyte seems like a logical path to continue experimentation. Unfortunately, as discussed in the theory section, suitable electrolyte materials are somewhat scarce, besides: designing electrolyte solutions is mostly part of the discipline of chemistry than of physics due to the background knowledge needed. It is possible however to change the surface properties of an electrolyte (e.g. SEI layer formation), without changing it's bulk behaviour (conductivity, viscosity).[63]

Komaba *et al.*[64] experimented with the addition of Mn(II) to EC-DEC electrolyte to enhance the cycle life of a Li-$LiMn_2O_4$ battery with positive results. An experiment by Wrodnigg *et al.*[63] involved adding ethylene sulfite (ES, $C_2H_4O_3S$, see 5.1) to EC and PC (propylene carbonate) electrolyte in a Li-$LiMn_2O_4$ battery.

5.4. Organic additives

Introducing elements into the electrolyte that will form an SEI layer with silicon before the native electrolyte compounds will do so can result in a more stable SEI layer. Addition of fluorethylene carbonate (FEC) for example, has reduced the porosity of the SEI layer, reducing capacity loss during power

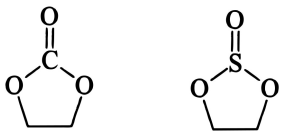

Figure 5.1: Structure of the ES (left) and EC molecules show their similarities. Source: Wrodnigg *et al.* [63]

cycling.[65] The SEI layer formed in presence of FEC is thinner and more concentrated on the surface, than the SEI layer formed in conventional EC electrolyte. During volume expansion, the FEC-SEI layer will be under less stress resulting in less cracks and better capacity retention.[39]

A Appendix

A.1. Detailed magnetron sputtering parameters

Power	150W DC
Sputtering rate	1.1 Å/s
Substrate temperature	Room temperature (293 K)
Gas	Argon
Gas flow rate	20 SCCM
Base pressure	$1.1 \cdot 10^{-7}$ Pa
Sputtering system	AJA ATC Series

A.2. V-t discharge curves

The following figures are the discharge curves for the cycled samples. From these curves the capacity curves were calculated.

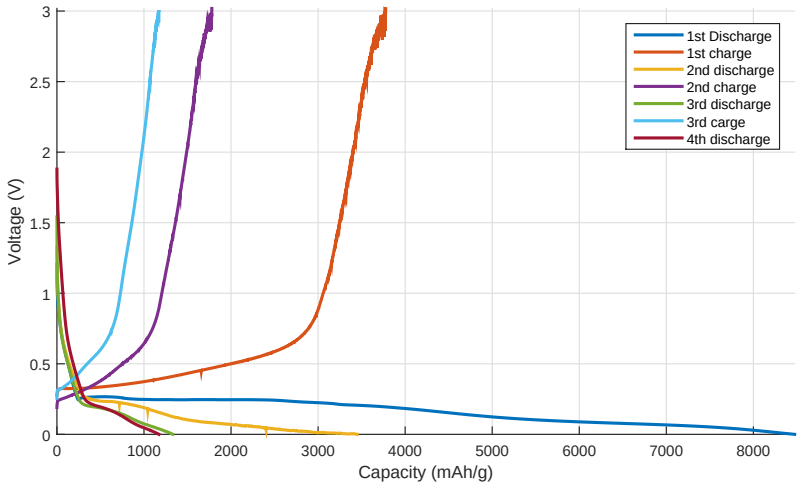

Figure A.1: Multiple cycle charge-discharge plot for the sample shown in figure 3.5.

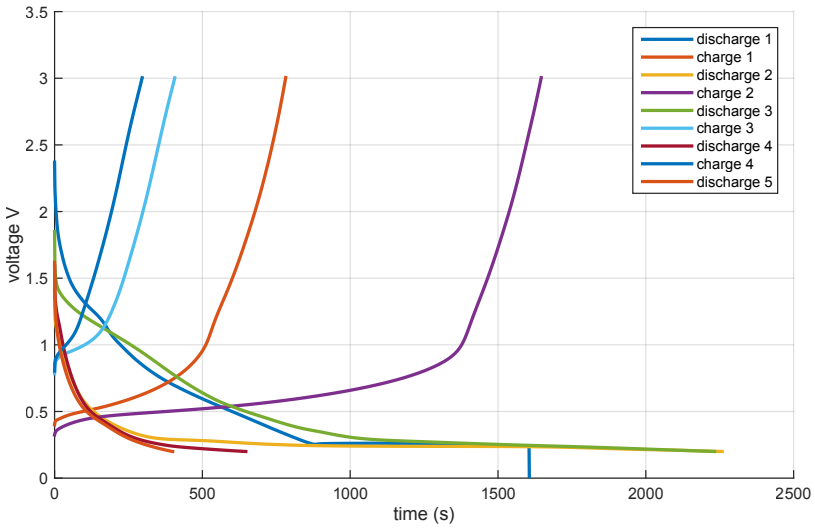

Figure A.2: Charge-discharge plot for a sample cycled between 3 and 0.2 V.

A.3. EELS spectrum

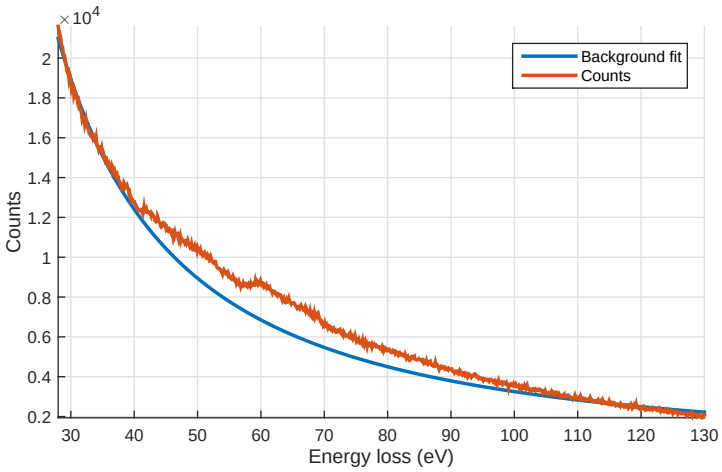

Figure A.3: EELS spectrum for a spot in the silicon layer.

A.4. EDX mapping data

The following data is supplementary to the EELS mapping of silicon and oxygen in figure 3.15.

A.4.1. Full view

The data below was captured in the area as shown in figure A.4.

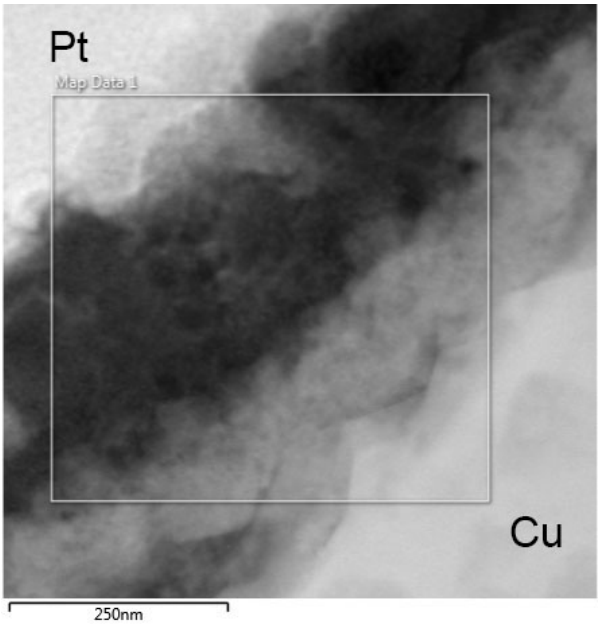

Figure A.4: STEM image of the area were the EDX mapping of the full height of the silicon layer was done.

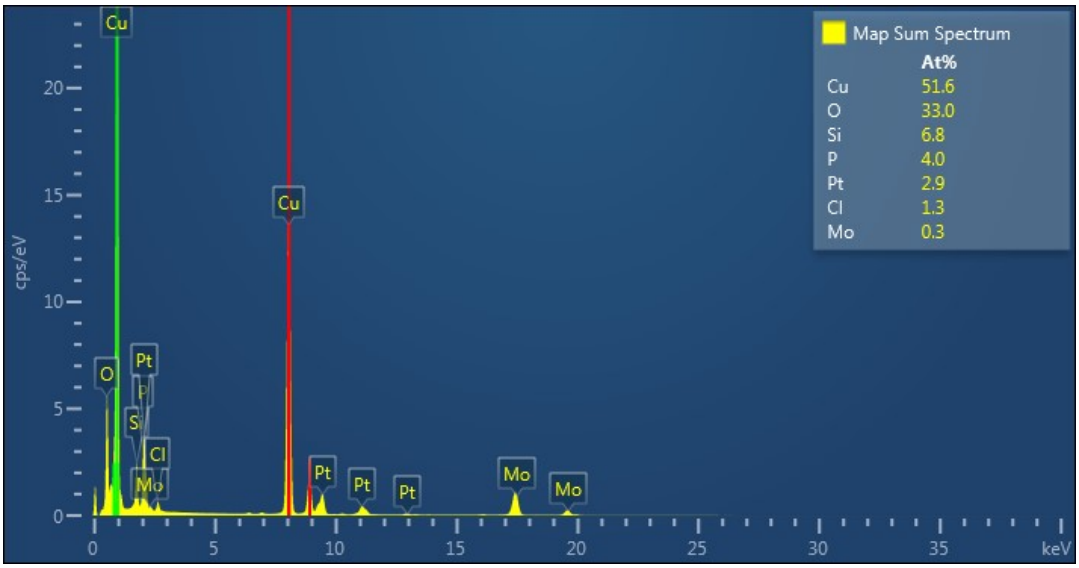

A.4.2. Detail view

The following data was captured from the detail view of the unlithiated Si layer as shown in figure A.5.

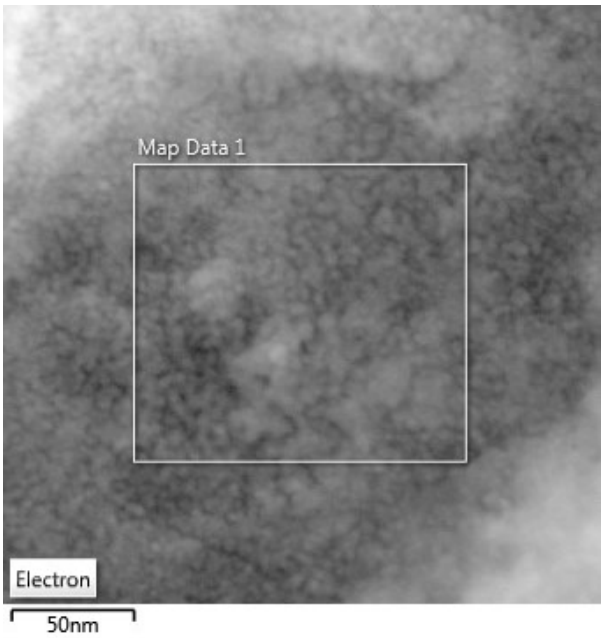

Figure A.5: STEM from the analysed area and marking of the mapped area.

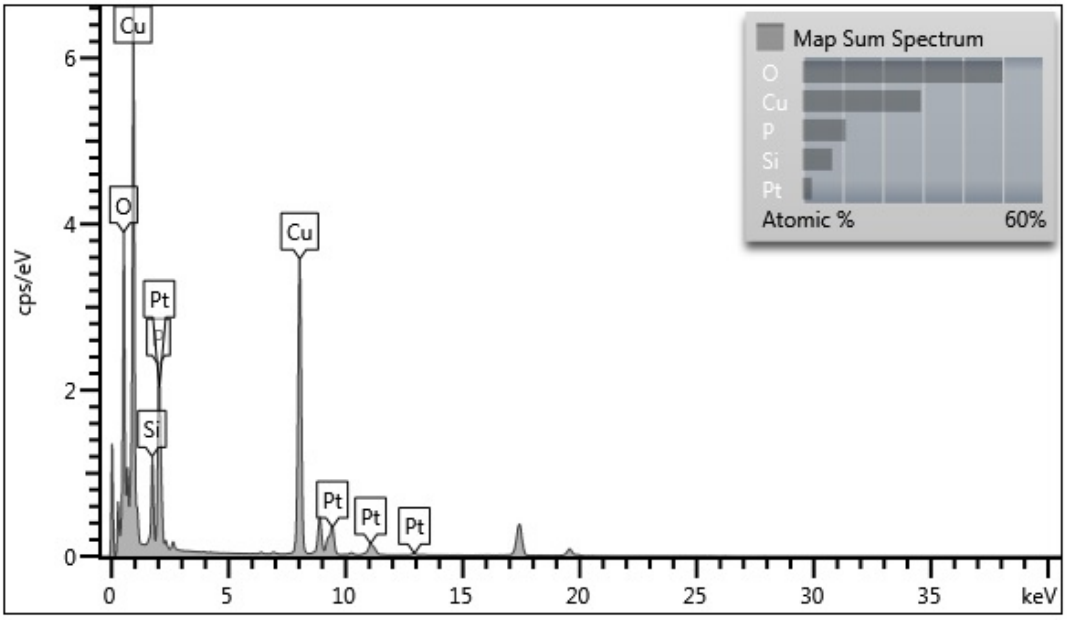

Figure A.6: EDX mapping spectrum for the entire mapped area.

A.5. STEM images from ion milled silicon discs

The STEM micrographs in this section were captured of a charged sample as described in section 4.1

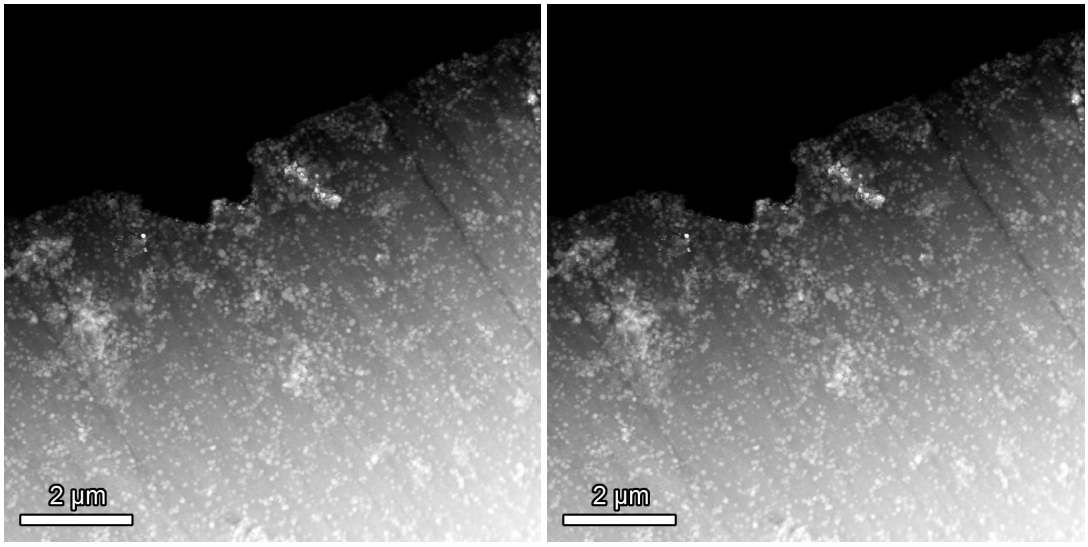

Figure A.7: STEM images at medium magnification of a lithiated silicon disc sample.

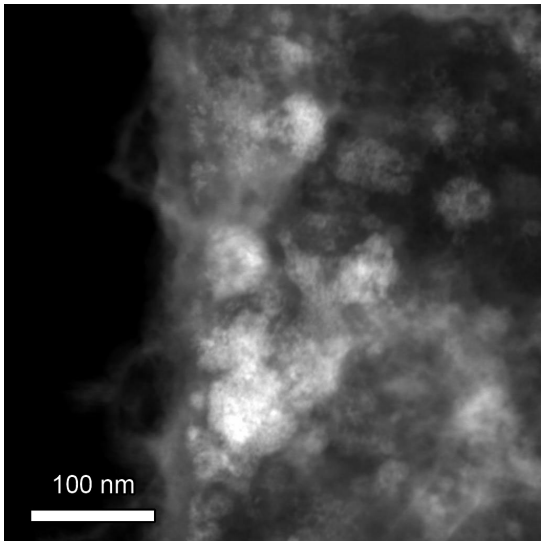

Figure A.8: Higher magnification STEM image of the lithiated silicon disc sample

Bibliography

[1] A. Jogalekar, *Moore's law and battery technology: No dice,* Online (2013).

[2] R. Brodd, K. Bullock, R. Leising, R. Middaugh, J. Miller, and E. Takuechi, *Batteries, 1977 to 2002,* Journal of the Electrochemical Society **151**, K1 (2004).

[3] J. Tarascon and M. Armand, *Issues and challenges facing rechargeable lithium batteries,* Nature **414**, 359 (2011).

[4] G. Nazri and G. Pistoia, eds., *Lithium Batteries - Science and Technology* (Kluwer Academic Publishers, 2004).

[5] M. Wakihara and O. Yamamoto, eds., *Lithium Ion Batteries - Fundamental and Performance* (Wiley-VCH, 1998).

[6] J. Goodenough and K. Park, *The li-ion rechargeable battery: A perspective,* Journal of The American Chemical Society **135**, 1167 (2013).

[7] M. Whittingham, *Chemistry of intercalation compounds: Metal guests in chalcogenide hosts,* Progress in Solid State Chemistry **12**, 41 (1978).

[8] M. Whittingham, *Electrical energy storage and intercalation chemistry,* Science **192**, 1126 (1976).

[9] K. Mizushima, P. Jones, P. Wiseman, and J. Goodenough, *Lixcoo2 (0<x<-1): A new cathode material for batteries of high energy density,* Materials Research Bulletin **15**, 783–789 (1980).

[10] A. K. Padhi, K. Nanjundaswamy, and J. Goodenough, *Phospho-olivines as positive-electrode materials for rechargeable lithium batteries,* Journal of The Electrochemical Society **144**, 1188 (1997).

[11] S. Levine, *The man who brought us the lithium-ion battery at the age of 57 has an idea for a new one at 92,* online (2015).

[12] Sony, *Corporate info,* Online.

[13] S. Bourderau, T. Brousse, and D. Schleich, *Amorphous silicon as a possible anode material for li-ion batteries,* Journal of Power Sources **81-82**, 233 (1999).

[14] J. St. John, *Amprius gets usd 30m boost for silicon-based lithium-ion batteries,* Online (2014).

[15] I. Buchmann, *Batteries in a Portable World: A Handbook on Rechargeable Batteries for Non-Engineers*, 3rd ed. (Cadex Electronics Inc., 2011).

[16] T. Bandhauer, S. Garimella, and T. Fuller, *A critical review of thermal issues in lithium-ion batteries,* Journal of The Electrochemical Society **158**, R1 (2011).

[17] B. Kang and G. Ceder, *Battery materials for ultrafast charging and discharging,* Nature **458**, 190 (2009).

[18] A. Andriiko, P. Rudenok, and L. Nyrkova, *Diffusion coefficient of li+ in solid-state rechargeable battery materials,* Journal of Power Sources **72**, 146 (1998).

[19] IHS Engineering360, *Potentiostats and galvanostats information on globalspec,* Online (2015).

[20] D. Aurbach, B. Markovsky, A. Shechter, Y. Ein-Eli, and H. Cohen, *A comparative study of synthetic graphite and li electrodes in electrolyte solutions based on ethylene carbonate-dimethyl carbonate mictures,* Journal of The Electrochemical Society **143**, 3809 (1996).

[21] J. Goodenough and Y. Kim, *Challenges for rechargeable lithium batteries,* Chemistry of Materials **22**, 587 (2010).

[22] D. Aurbach, E. Zinigrad, Y. Cohen, and H. Teller, *A short review of failure mechanisms of lithium metal and lithiated graphite anodes in liquid electrolyte solutions,* Solid State Ionics **148**, 406 (2002).

[23] C. Daniel and J. Besenhard, *Handbook of Battery Materials*, edited by C. Daniel and J. Besenhard (Wiley-VCH, 2011).

[24] S. Lux, J. Chevalier, I. Lucas, and R. Kostecki, *Hf formation in lipf6-based organic carbonate electrolytes,* ECS Electrochemistry Letters **2**, A121 (2013).

[25] J. Besenhard and M. Winter, *Advances in battery technology: Rechargeable magnesium batteries and novel negative-electrode materials for lithium ion batteries,* ChemPhysChem **3**, 155=159 (2002).

[26] A. Mukhopadhyay and B. Sheldon, *Deformation and stress in electrode materials for li-ion batteries,* Progress in Materials Science **63**, 58 (2014).

[27] T. Yoon, S. Park, J. Mun, J. Ryu, W. Choi, and Y. Kang, *Failure mechanisms of $LiNi_0 \cdot 5 Mn_1 \cdot 5 O_4$ electrode at elevated temperature,* Journal of Power Sources **215**, 312 (2012).

[28] M. Pinson and M. Bazant, *Theory of sei formation in rechargeable batteries: Capacity fade, accelerated aging and lifetime prediction,* (2012), arXiv:1210.3672.

[29] P. Arora and R. White, *Capacity fade mechanisms and side reactions in lithium-ion batteries,* Journal of the Electrochemical Society **145**, 3647 (1998).

[30] R. Fong, U. von Sacken, and J. Dahn, *Studies of lithium intercalation into carbons using nonaqueous electrochemical cells,* Journal of the Electrochemical Society **137**, 2009 (1990).

[31] D. Li, D. Danilov, Z. Zhang, H. Chen, and Y. Yang, *Modeling the sei-formation on graphite electrodes in lifepo4 batteries,* Journal of The Electrochemical Society **162**, A858 (2015).

[32] H. Wu, G. Chan, J. Choi, I. Ryu, Y. Yao, M. McDowell, S. Lee, A. Jackson, Y. Yang, L. Hu, and Y. Cui, *Stable cycling of double-walled silicon nanotube battery anodes through solid–electrolyte interphase control,* Nature Nanotechnology **7**, 310–315 (2012).

[33] S. Kim, A. Van Duin, and V. Shenoy, *Effect of electrolytes on the structure and evolution of the solid electrolyte interphase (sei) in li-ion batteries: A molecular dynamics study,* Journal of Power Sources **196**, 8590 (2011).

[34] R. Sacci, J. Black, N. Balke, N. Dudney, and K. More, *Nanoscale imaging of fundamental li battery chemistry: Solid-electrolyte interphase formation and preferential growth of lithium metal nanoclusters,* Nano Letters **15**, 2011 (2015).

[35] S. Zhang, *A review on electrolyte additives for lithium-ion batteries,* Journal of Power Sources **162**, 1379 (2006).

[36] D. Aurbach, *Review of selected electrode–solution interactions which determine the performance of li and li ion batteries,* Journal of Power Sources **89**, 206 (2000).

[37] M. McArthur, S. Trussler, and J. Dahn, *In situ investigations of sei layer growth on electrode materials for lithium-ion batteries using spectroscopic ellipsometry,* Journal of The Electrochemical Society **159**, A198 (2012).

[38] C. Khan, R. Ruffo, S. Sae Hong, and Y. Cui, *Surface chemistry and morphology of the solid electrolyte interphase on silicon nanowire lithium-ion battery anodes,* Journal of Power Sources **189**, 1132 (2009).

[39] M. Nie, D. Abraham, Y. Chen, A. Bose, and B. Lucht, *Silicon solid electrolyte interphase (sei) of lithium ion battery characterized by microscopy and spectroscopy,* The Journal of Physical Chemistry C **117**, 13403–13412 (2013).

[40] J. Lei, L. Li, R. Kostecki, R. Muller, and F. McLarnon, *Characterization of sei layers on limn2o4 cathodes with in situ spectroscopic ellipsometry,* Journal of The Electrochemical Society **152**, A774 (2005).

[41] A. Andersson, A. Henningson, H. Siegbahn, U. Jansson, and K. Edström, *Electrochemically lithiated graphite characterised by photoelectron spectroscopy,* Journal of Power Sources **119-121**, 522 (2003).

[42] J. Li and J. Dahn, *An in situ x-ray diffraction study of the reaction of li with crystalline si,* Journal of The Electrochemical Society **154**, A156 (2007).

[43] T. Takamura, M. Uehara, J. Suzuik, K. Sekine, and K. Tamura, *High capacity and long cycle life silicon anode for li-ion battery,* Journal of Power Sources **158**, 1401 (2006).

[44] M. Park, M. Kim, J. Joo, K. Kim, J. Kim, S. Ahn, Y. Cui, and J. Cho, *Silicon nanotube battery anodes,* Nano Letters **9**, 3844 (2009).

[45] H. Jung, M. Park, Y. Yoon, G. Kim, and S. Joo, *Amorphous silicon anode for lithium-ion rechargeable batteries,* Journal of Power Sources **115**, 346 (2003).

[46] Z. Popov, A. Fedorov, A. Kuzubov, and T. Kozhevnikova, *A theoretical study of lithium absorption in amorphous and crystalline silicon,* Journal of Structural Chemistry **52**, 861 (2011).

[47] M. Obrovac and L. Christensen, *Structural changes in silicon anodes during lithium insertion/extraction,* Electrochemical and Solid-State Letters **7**, A93 (2004).

[48] M. T. McDowell, S. W. Lee, J. T. Harris, B. A. Korgel, C. Wang, W. D. Nix, and Y. Cui, *In situ tem of two-phase lithiation of amorphous silicon nanospheres,* Nano Letters **13**, 758 (2013), pMID: 23323680, http://dx.doi.org/10.1021/nl3044508 .

[49] C. Ding, H. Zhang, X. Li, T. Liu, and F. Xing, *Vanadium flow battery for energy storage: Prospects and challenges,* The Journal of Physical Chemistry Letters **4**, 1281 (2013).

[50] Gringer, *Scheme tem en,* Online (2009).

[51] Australian Microscopy & Microanalysis Research Facility, *Diffraction patterns,* Online ().

[52] Australian Microscopy & Microanalysis Research Facility, *Background information - what is energy dispersive x-ray spectroscopy?* Online ().

[53] L. Giannuzzi and F. Stevie, *A review of focused ion beam milling techniques for tem specimen preparation,* Micron **30**, 197 (1999).

[54] S. Lux, I. Lucas, E. Pollak, S. Passerini, M. Winter, and R. Kostecki, *The mechanism of {HF} formation in lipf6 based organic carbonate electrolytes,* Electrochemistry Communications **14**, 47 (2012).

[55] M. Obrovac and L. Krause, *Reversible cycling of crystalline silicon powder,* Journal of The Electrochemical Society **154**, A103 (2007).

[56] E. Klaassen, K. Petersen, J. Noworolski, J. Logan, N. Maluf, J. Brown, C. Storment, W. McCulley, and G. Kovacs, *Silicon fusion bonding and deep reactive ion etching: a new technology for microstructures,* Sensors and Actuators **52**, 132 (1996).

[57] F. Laermer and A. Schilp, *Method of anisotropically etching silicon,* (1993), uS Patent 5,501,893.

[58] B. Wu, A. Kumar, and S. Pamarthy, *High aspect ratio silicon etch: A review,* Journal of Applied Physics **108**, 051101 (2010).

[59] Oxford Instruments Plasma Technology, *The bosch process for etching micro-mechanical systems (mems) - principles, advances and applications,* Online (2013).

[60] Pgalajda, Wikimedia Commons, *Bosch process sidewall,* Online (2005).

[61] MEMSnet, *Etching processes,* Online.

[62] Y.-C. Yen, S.-C. Chao, H.-C. Wu, and N.-L. Wu, *Study on solid-electrolyte-interphase of si and c-coated si electrodes in lithium cells,* Journal of The Electrochemical Society **156**, A95 (2009).

[63] G. Wrodnigg, J. Besenhard, and M. Winter, *Ethylene sulfite as electrolyte additive for lithium-ion cells with graphitic anodes,* Journal of The Electrochemical Society **146**, 470 (1999).

[64] S. Komaba, B. Kaplan, T. Ohtsuka, Y. Kotaoka, N. Kumagai, and H. Groult, *Inorganic electrolyte additives to suppress the degradation of graphite anodes by dissolved mn(ii) for lithium-ion batteries,* Journal of Power Sources **119-121**, 378 (2003).

[65] N. Choi, K. Yew, K. Lee, M. Sung, H. Kim, and S. Kim, *Effect of fluoroethylene carbonate additive on interfacial properties of silicon thin-film electrode,* Journal of Power Sources **161**, 1254 (2006).